Universidad Nacional de Colombia - Sede Medellín

# SIMULATION TOOLBOX FOR IN-SITU COMBUSTION APPLIED TO EXPERIMENTAL SETUPS.

*Author:*
Juan Felipe Hincapié Álvarez

*Advisor:*
Alejandro Molina

*Thesis presented as a partial requirement to obtain the degree of:*
*M.Sc. in Chemical Engineering*

Research Group: Bioprocesos y Flujos reactivos
Facultad de Minas, Departamento de Procesos y Energía

Medellín, Colombia
2016

UNIVERSIDAD NACIONAL DE COLOMBIA - SEDE MEDELLÍN

# *Abstract*

Facultad de Minas

Facultad de Minas, Departamento de Procesos y Energía

M.Sc. in Chemical Engineering

**SIMULATION TOOLBOX FOR IN-SITU COMBUSTION APPLIED TO EXPERIMENTAL SETUPS.**

by Juan Felipe Hincapié Álvarez

A simulation Toolbox, exclusively designed for the analysis of different experimental setups for in-situ combustion (ISC) analysis, was developed. This Toolbox can be targeted for the analysis of chemical kinetics. The models in the Toolbox are based on fundamental conservation laws, physical correlations for porous media properties and property databases available in the open literature. The Toolbox, written in Matlab, is coupled to CANTERA, a software for the analysis of complex chemical mechanisms and thermodynamics for gas phase reactions.

The toolbox considers three main applications: kinetic cell, plug flow reactor and combustion tube. Each one can be applied to the analysis of different issues in ISC experiments, as illustrated throughout the thesis. The kinetic cell module, as its name indicates, is particularly suitable for the analysis of these experimental setups. It includes the ability to follow gas phase reactions. This module is used with the GRI-Mech 3.0, a complex reaction mechanism originally designed to model natural gas combustion, that includes 325 reactions and 53 species to address the existence of CO oxidation in the gas phase of ISC experiments. The plug flow reactor module, modeled as a series of kinetic cells, simplifies computation and is suitable for the design of experiments that reduce the existence of concentration gradients in a kinetic cell. The last module can model a combustion tube including Darcy's flow and fundamentals of flow in porous media. It captures important phenomena such as oil plugging as it includes pressure balance, based on volume conservation principles and thermodynamic relations. The analysis with these three modules represents an ideal complement to reservoir modeling software that, while suitable for the study of oil production in field has not been designed for the complex processes that take place in in-situ combustion experiments.

# *Acknowledgements*

First of all, I would like to thank my advisor Prof. Alejandro Molina for his guidance, critical feedback and for allow me to develop my research with intellectual freedom. His thoroughness and the way of face the problems have contributed significantly to my professional growth.

I would like to say thanks to the valuable feedback and interactions with Stanford University Research Group (SUPRI-A), especially to Prof. Anthony Kovscek and Prof. Louis Castanier. I am also very thankful with Luiz Sampaio and Folake Ogunbanwo for all the collaboration and discussions during my internship at Stanford.

I also highlight the financial support from "Jovenes investigadores, convocatoria 566 de 2012" and the project of Colciencias-Ecopetrol "Caracterización Mediante Técnicas Láser de las Reacciones Químicas de Petróleo Crudo Durante Combustión In-Situ" with contract RC. No. 0264 2013.

I owe my life, my efforts and all my goals to my family Juan F. Hincapié, Luz A. Álvarez and Daniel A. Hincapié, but also an especial acknowledgement to my girlfriend Ana C. Restrepo, with her knowledge in chemical engineering, motivation and support this thesis would not be possible.

Finally, no study would be complete without the support of the colleagues and friends from the Colombian research group: Bioprocesos y Flujos Reactivos. I wish to record my gratitude to the following: Juan Jose Arias, Juan David Alzate, Juan Esteban Duque, Sandra López, Noel Gómez and Amérika Arévalo.

# Contents

# List of Figures

# List of Tables

# Abbreviations

| | |
|---|---|
| **EOR** | **E**nhenced **O**il **R**ecovery |
| **HTO** | **H**igh **T**emperature **O**xidation |
| **ISC** | **I**n **S**itu **C**ombustion |
| **LTO** | **L**ow **T**emperature **O**xidation |
| **RTO** | **R**amped **T**emperature **O**xidation |
| **SARA** | **S**aturate **A**romatic **R**esins **A**sphaltenes |
| **CDS** | **C**entral **D**ifference **S**cheme |
| **CMG** | **C**omputer **M**odelling **G**group |
| **CFD** | **C**omputational **F**luid **D**ynamics |
| **NDF** | **N**umerical **D**ifferentiation **F**ormulas |
| **SATP** | **S**tandard **A**mbientic **T**emperature and **P**ressure 298.15 K and 101.13kPa |
| **TGA** | **T**hermal **G**ravimetric **A**nalysis |
| **OOIP** | **O**riginal **O**il **I**n **P**lace |
| **LPG** | **L**iqufied **P**etroleum **G**as |
| **SAGD** | **S**team **A**ssisted **G**ravity **D**rainage |

# Physical Constants

| | | | |
|---|---|---|---|
| Gravity | $g$ | $=$ | $9.81\ m\ s^{-2}$ |
| Gas constant | $R$ | $=$ | $8.314\ m^3\ Pa\ K^{-1}\ mol^{-1}$ |

# Symbols

| | | |
|---|---|---|
| $a_i$ | Activity coefficient | |
| $A_j$ | Frequency factor | *Depends on the reaction* |
| $C_i$ | Concentration | $mol \cdot m^{-3}$ |
| $Cp$ | Heat capacity | $J \cdot mol^{-1} \cdot K^{-1}$ |
| $Ea_j$ | Activation energy | $J \cdot mol^{-1}$ |
| $D$ | Depth | $m$ |
| $f_{i,j}$ | Phase fugacity | $Pa$ |
| $F_i$ | Molar flow rate | $mol \cdot min^{-1}$ |
| $h$ | Enthalpy | $J \cdot mol^{-1}$ |
| $h_j$ | Enthalpy of phase j | $J \cdot mol^{-1}$ |
| $i$ | Especies oil, water, CO, $CO_2$, $N_2$, $O_2$... | |
| $j$ | Phases oil, water, gas and solid | |
| $J_i$ | Molar flux | $mol \cdot m^{-2}\ min^{-1}$ |
| $k$ | Permeability | *Darcy* |
| $k_e$ | Effective permeability | *Darcy* |
| $k_{rj}$ | Relative permeability | |
| $K_i$ | Equilibrium constant k-value | |
| $m_i$ | Mass of specie i | $g$ |
| $nc$ | Number of species | |
| $neq$ | Number of equations | |
| $nP$ | Number of phases | |
| $nR$ | Number of reactors or nodes | |
| $nt$ | Number of times | |
| $N_i$ | Moles of specie i | *mole* |
| $P$ | Pressure | $Pa$ |

| | | |
|---|---|---|
| $P_{g,i}$ | Partial pressure | $Pa$ |
| $q_h$ | Thermal sinks and sources | $J \cdot min^{-1}$ |
| $q_i$ | Source/sink molar | $mol \cdot min_{-1}$ |
| $\widehat{q_i}$ | Source/sink, molar flux | $mol \cdot min^{-1}$ |
| $Q^{conv}$ | Heat flux - convection. | $J \cdot min^{-1}$ |
| $Q^{cond}$ | Heat flux - conduction. | $J \cdot min^{-1}$ |
| $Q^{ext}$ | Heat flux - furnace. | $J \cdot min^{-1}$ |
| $R$ | Ideal gas constant | $m^3 \cdot Pa \cdot mol^{-1} \cdot K^{-1}$ |
| $S$ | Saturation | |
| $t$ | Time | $min$ |
| $T$ | Temperature | $K$ |
| $u_j$ | Darcy Velocity - phase j | $m \cdot min^{-1}$ |
| $U_j$ | Internal energy - phase j | $J \cdot mol^{-1}$ |
| $U$ | Overall heat transfer coefficient | $W \cdot K^{-1} \cdot m^{-2}$ |
| $v$ | Molar volume | $m^3 \cdot mol^{-1}$ |
| $V$ | Volume | $m^3$ |
| $V_{cell}$ | Volume of cell | $m^3$ |
| $V_p$ | Porous volume | $m^3$ |
| $V_b$ | Block volume | $m^3$ |
| $W$ | Molecular weight | $g \cdot mol^{-1}$ |
| $x_i$ | Liquid mole fraction | |
| $X, Y, Z$ | Cartesian coordinates | $m$ |
| $y_i$ | Gas mole fraction | |
| $Z_i$ | Overall molar fraction of specie i | |
| $\widehat{c}_f$ | Average fluid compressibility | $Pa^{-1}$ |
| $\widehat{c}_R$ | Average rock compressibility | $Pa^{-1}$ |
| $\widehat{c}_T$ | Average thermal expansion coefficient | $K^{-1}$ |
| $\alpha$ | Thermal conductivity | $J \cdot m^{-1} \cdot min^{-1} \cdot K^{-1}$ |
| $\gamma^j$ | Reaction rate | $mole \cdot min^{-1}$ |
| $\Delta H_{rxn}$ | Reaction enthalpy | $J \cdot mol^{-1}$ |
| $\Lambda^{ij}$ | Stoichiometric matrix | |
| $\theta$ | Heating rate | $K \cdot min^{-1}$ |
| $\mu_j$ | Viscosity of phase j | $Pa \cdot min$ |

| | | |
|---|---|---|
| $\xi$ | Vector of variables for all nodes | |
| $\dot{\xi} i$ | Vector with the derivatives | |
| $\xi_k$ | Vector for variables for node k | |
| $\xi_{sol}$ | Solution matrix | $[nt, neq]$ |
| $\rho_j$ | Phase molar density | $mol \cdot m^{-3}$ |
| $\Psi$ | Vapor fraction, flash calculation | |
| $\Omega$ | Control volume | $m^3$ |
| $\tau$ | Residence time | $min$ |
| $\upsilon_i$ | Molar volume | $m^3 \cdot mol^{-1}$ |
| $\phi$ | Porosity | |
| $\phi_i, \widehat{\phi}_i, \phi_i^{sat}$ | Fugacity coefficients | |

# Research problem

In situ combustion (ISC) is an enhanced oil recovery process(EOR) that is usually referred as a thermal recovery method, where the air is injected to the reservoir to burn a fraction of the crude oil. Exothermic reactions, particularly coke combustion, increase the temperature in the process that allows fluids flow due to an important reduction of their viscosities [1].

Combustion of the crude oil in porous media is a complex process that has not been completely understood. This complexity is given by the difference in scale (laboratory to the field) and the unknown phenomena such as chemical reaction pathway, mass transfer, the heterogeneity of the rock formation, geomechanical issues, phase equilibrium, heat losses, and other aspects that do not allow a good implementation of pilot projects in field [2–5].

Current research topics for in situ combustion have focused on understanding the behavior of chemical reactions, because they are an important part of the changes in the reservoir. Combustion of crude oil determines the released heat, the amount of coke deposition (affecting the porosity), the type and amount of produced gases [6, 7].

Combustion tubes and kinetic cells are the experimental setups most widely used to characterize ISC. The purpose of the combustion tube is to emulate in laboratory scale the combustion front, taking into account the behavior of the coupled phenomena of fluid dynamic and chemical reaction. The kinetic cell is mostly used to study the reactions that take place in the ISC process [8]. Some studies have developed mechanisms and reaction kinetics, mostly for bitumen and heavy oil from Canada, is the case for the simplified model proposed by [9] and a more detailed model based on SARA fractions (Saturates, Aromatics, Resins and Asphaltenes) as used by [1] in their study.

Kinetic cells have been modeled as a perfectly mixed semi-batch reactor where the stationary mixture of oil and rock reacts with the air that flows through the reactor. However, many researchers observed heterogeneities, causing different reaction velocities along the cell [10–12]. Thus, chemical kinetics can be controlled by mass transfer and segregation phenomena that the model does not consider, so the kinetic parameters

should be evaluated in a model that accurately represents the process, instead of usually calculated models of ideal reactors (batch or semi-batch).

On the other hand, combustion tubes are usually modelled as a simple one-dimensional reactor. This assumption works accurately well for small laboratory setups, where the radial effects and heat losses are negligible. But the model cannot represent all the complex behaviour in the reservoir conditions.

As mentioned above, the modeling of in-situ combustion has many challenges in properly considering all the complexity of the process. Aditionally, modeling a single experimental setup does not allow versatility in the study of the process. The simulation toolboxes have a big potential regarding the design of experiments, as they guarantee a similar assembly, that makes possible to evaluate different ways to model the process. They also allow to study different parametric sensitivity to predict problems in the design or in the experimental setup. The models can be also applied to determine the optimal experimental conditions and to adjust physical correlations [13]. Therefore, it is necessary to implement a reliable tool to represent and predict the performance of the ISC process to make better decisions in the operation design.

# Research objectives

## Overall objetive

To develop an ISC Simulation Toolbox to predict the behavior of the process on experimental setups.

## Specific objetives

- To formulate a mathematical set of equations that describes the reactive flow in porous media.
- To perform a sensitivity study of parameters and operating conditions for experimental setups.
- To apply numerical methods and algorithms to build the Simulation Toolbox, which suits the design alternatives.

# Chapter 1

# Introduction

The purpose of this chapter is to demonstrate the industrial applicability of the in situ combustion process and to illustrate the importance of lab scale experiments on its study. Also the main theoretical fundamentals of the process and definitions of the variables are presented.

## 1.1 Theoretical framework

### 1.1.1 Enhanced oil recovery

Traditionally, oil recovery operations have been subdivided as primary, secondary and tertiary. During primary recovery stage, the natural pressure of the reservoir is enough to force the production from well to the surface, also natural gas production occurs [14, 15]. When the pressure in reservoir cannot drive the fluid flow and production declines, another method should be implemented. In secondary recovery stage, the injection of fluids like water (Waterflood) and immiscible gases, increases reservoir pressure in order to sweep out the oil. At this step, primary and secondary production can offer from 35 to 50% OOIP (original oil in place), depending of the physical properties of fluids (such as density and viscosity) and reservoir conditions. Tertiary production use miscible gases, chemicals and heat transfer to improve production of the remaining oil after secondary recovery. The interaction of the injected fluid with the reservoir allows different mechanisms for fluid flow such as viscosity reduction or wettability modification [16].

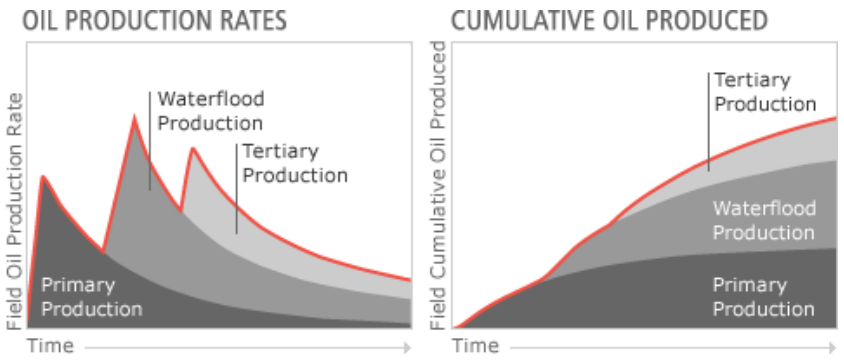


FIGURE 1.1: Oil recovery stages [17].

Figure 1.1 presents the oil production rate and cumulative oil produced for the main oil recovery stages. When primary production becomes difficult, the oil production rate decreases, then a secondary recovery method improves the production rate. Finally, when secondary recovery does not reach the expected production rate a tertiary stage (enhanced oil recovery) is required. It is important to note that the difficulty of the extraction and the process cost, grow as oil production increases.

However, heavy oils have been changing the paradigm for oil recovery, because it is in most of the cases expensive to start production as a chronological sequence as mentioned before. Heavy oils are not conducted in the specified order, because if the oil is sufficiently viscous, it may not flow at primary or secondary conditions and thermal recovery might be the only way to recover a significant amount of oil. A classification based on process description and reservoir condition is more useful than chronological sequences.

Tertiary recovery, or a more accepted term "Enhanced oil recovery methods", increase the mobility of the crude oil with different kind of technologies, which can be classified into five categories: mobility control, chemical agents, miscible gas injection, thermal recovery and special cases such microbial injection.

Mobility control processes as polymer waterflood and some chemical agents as surfactants are designed to change mobility ratios with the oil- water bank and to decrease the surface tension. These techniques allow a more uniform volumetric sweep and, in the case of polymer injection, is possible to avoid the free paths (finger paths) of the water to the production well, because the polymer solution mobility is less than water mobility. The injection of surfactants to reservoirs have been used to reduce residual oil

saturation by surface tension mechanisms. It is common to combine the polymer injection with surfactants in order to have a better performance of the operation. However, besides the high cost of the chemicals, there are some technical difficulties with this kind of methods such as sensitivity to salinity concentration and adsorption on the porous media, reducing the amount of the component in solution and decreasing the effective permeability [18].

On the other hand, miscible gas injection such as $CO_2$ and Liquefied Petroleum Gas (LPG) are commonly used to displace oil in a single phase with a lower viscosity than the original condition. Phase equilibrium is also important in this process, because the miscibility of the gas in the liquid phase is controlled by temperature, pressure and composition. Difficulties such as high pressure and viscous fingering of the gas results in a challenging operation [14, 15]. Nevertheless, injection of $CO_2$ can be also a good option if the gas is produced by cogeneration or other processes on the field.

Thermal recovery methods like steam injection or in-situ combustion are used to heat the crude oil, achieving significant viscosity reduction. Some techniques of steam injection are cyclic stimulation and Steam Assisted Gravity Drainage (SAGD). The advantages of the steam are the high heat capacity and latent heat, on a per unit mass basis, steam carries more heat than any other industrial fluid. Also, it is possible to perform cogeneration with the steam and get electricity for low pressure operations [19]. The limitations of these methods are related to wellbore heat losses in deep reservoirs (more or less 5000 ft) and surface operation control. On the other hand, combustion has a big potential in cases where steam injection is not possible to operate. It is a complex but very effective technique, because the heat is generated inside the reservoir and water is not required in large amounts [7]. Also, combustion carries out mechanism from the other methods as gas drive and steam generation.

The understanding of the chemical reactions for in situ combustion process is a real challenge. To get reliable results, synergy between different experimental tests for lab scale research is absolutely necessary to get all the parameters to scale the process to field applications [20].

As a definition in this thesis, the classification of heavy oil given by Banerjee is shown as follows [21]:

- Heavy oil: API gravity between 10° - 21° and viscosity between 10 cP – 1000 cP.
- Extra Heavy oil: API gravity less than 10° and viscosity between 1000 cP – 10,000 cP.
- Tar Sands and Bitumen: API gravity less than 10° and viscosity greater than 10,000 cP.

### 1.1.2 In-situ combustion process

In-situ combustion or fireflooding (movement of a burning front), was patented in 1923 by Wolcott and Howard in the United States, the first field pilot project was recorded in the old Soviet Union in 1933 [5]. Since 1950, research and field applications allows many ISC projects in operation like Rumanian fields [22]. However, the number of active commercial projects decreases, but research in laboratory and numerical simulation, have been increasing in recent years as Turta mentioned in his recent review paper [5]. Also this is a technically efficient and attractive process that has to be completely studied to turn into an economically viable option.

ISC is a thermal oil recovery technique where an oxidizing gas (air or air enriched with oxygen) is injected into oil reservoirs to generate heat by burning a fraction of the crude oil, forming a combustion front [6]. For heavy oils, ISC is a very appropriate technique due to the considerable reduction in oil viscosity with temperature increases. Furthermore, oil production is driven by flue gases and the increasing pressure, as consequence of chemical reactions [1].

It is important to notice that the HPAI process (High Pressure Air Injection) is often referred to deep light oil reservoirs, whereas in-situ combustion is commonly used for heavy oil reservoirs as Khansari clarified in his thesis [6].

In-situ combustion takes advantages over other thermal recovery methods, because the main energy required to displace the oil, is generated in the reservoir from the heat released by combustion reactions [23], thus heat losses are quite small at the wellbore. For very deep reservoirs this process has more advantages than steam injection, because in the latter the steam is generated at the surface and has to travel along the wellbore into the reservoir, resulting in important heat losses to the surroundings before it can reach the oil [7, 24].

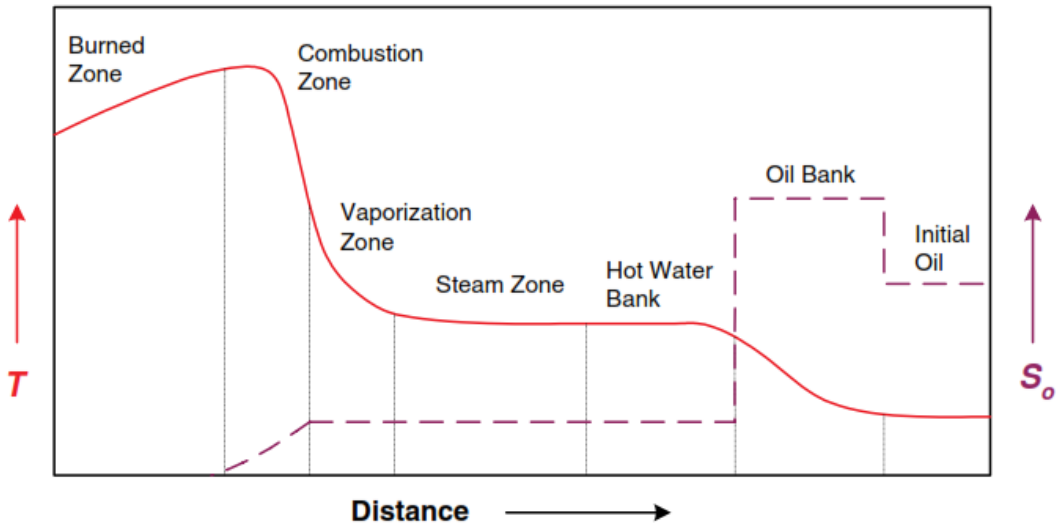


FIGURE 1.2: Forward combustion zones. Temperature and saturation profiles [13].

In brief, there are two methods of operation for ISC, based on the directions of air flow and combustion front propagation. When the combustion front advances in the same direction as the air flow and the ignition is located in the injection well, the process is usually named forward combustion. Whereas if the combustion front moves against the air flow and the ignition is located in the producing well, the process is reverse combustion.

Reverse combustion is an economically unattractive process, because more oxygen is required to propagate the combustion front due to the dispersive gas flow in the reservoir before the burning of the oil at the producing well [7]. Further, it is possible that the unreacted coke behind the combustion front starts to burn, reverting the process to the other way (forward combustion), then the operation turns uncontrollable even on laboratory experiments. For this reason the forward combustion is more attractive process and a more detailed description is presented.

As was mentioned by [24–26] in their works and also in Figure 1.2, for forward combustion, starting from the injection well, fresh air flows through the burned zone that is clean, due to the combustion front swept. The combustion zone has the highest temperature in the reservoir due to chemical reactions, where oxygen is consumed by hydrocarbons and the remaining coke to produce carbon oxides and water. In absence of oxygen, the zone adjacent to the combustion front is sufficiently hot to promote thermal cracking (or pyrolysis) and vaporization of volatile compounds, also coke generation in

this zone allows the process to be self-sustaining, because coke is the main fuel source for the combustion. The water from combustion and vaporization generates the steam zone or usually named steam plateau, also heat transfer to the surrounding oil and rock matrix enables the formation of another zone called hot water bank, where temperature decreases below saturation. Finally, the last zone in the process is the main volume of oil, where a fraction is heated by the water bank and the other has the original reservoir temperature. It is important to notice in Figure 1.2 the oil saturation difference between initial oil and oil bank due to fluid displacement.

There are two ways to carry out forward combustion, the first one is the previous definition (dry forward combustion), and other way is adding water to the injection (wet forward injection). For dry forward combustion, large part of the energy generated remains behind the combustion front as heat absorbed by the rock matrix. Thus when air flows through the burned zone, the heat is not transported efficiently due to the low heat capacity of gases [27]. Wet forward combustion provides water that can recover the remaining heat and it could be transferred to the oil bank, making a more defined temperature profile (as a peak) [13]. For dry forward combustion with a few initial reservoir water, the steam plateau zone is too small.

More sophisticated methods have been developed recently as "Toe to Heel Air Injection" or THAI process. The operation involves horizontal wells in which air is injected in a vertical well and oil is produced from a long horizontal well. So, the heated oil is drained whereas the combustion front advances [23, 25, 28].

### 1.1.3 Chemical reactions mechanisms

The chemical reactions and the coupled phenomena between oil and air are the most important parts for ISC. These chemical reactions do not only depend on the type of oil and rock properties, it is proved that the reactions can be influenced by clays and metallic catalysts on the rock matrix [6, 29]. Burger and Fassihi investigated the effects of matrix on the oxidation reactions [30, 31], they found that clays and fine sands enhance deposition of more fuel because of the adsorption characteristics on a higher surface area. Also in experiments with higher surface area and fuel dispersion the reactions were found to be kinetically controlled instead of diffusion controlled. Mamora studied the effect

of clays and fine sands, but also proposed a new analytical model that considers the variation of the reactions with surface area for oxygenated hydrocarbons as fuel [32].

There is an overall classification, widely accepted by the scientific community, which groups the reactions as follows: Low temperature oxidation (LTO), thermal cracking-pyrolysis and high temperature oxidation (HTO).

LTO is a gas/liquid heterogeneous pseudoreaction which generally operates in the temperature range below 350°C, it produces oxygenated compounds and a negligible amount of carbon oxides [33] It is possible to find some hydrocarbons such as alcohols, aldehydes, hydroperoxides, ketones, carboxylic acids and water as mentioned in these works [6, 34].

The HTO pseudoreaction is referred to the fuel combustion, in which the main products are carbon dioxide, carbon monoxide and water. The normal temperature is above 350°C and it is mainly characterized by a heterogeneous solid-gas reaction such as coke combustion. Moreover, this exothermic reaction is very important, because it provides the thermal energy to sustain and propagate the combustion front. A complete review and data about ISC features can be found in Sarathi's handbook [7]. The chemical reaction for hydrocarbons combustion at HTO regimen is given by:

$$\mathrm{CH}_n + \left[\frac{2m+1}{2(1+m)} + \frac{n}{4}\right]\mathrm{O}_2 \longrightarrow \left[\frac{m}{(1+m)}\right]\mathrm{CO}_2 + \left[\frac{1}{(1+m)}\right]\mathrm{CO} + \left[\frac{n}{2}\right]\mathrm{H}_2\mathrm{O} \qquad \text{(R1)}$$

where n is the atomic ratio of hydrogen and carbon and m is the molar ratio of produced $CO_2$ to CO (m equals zero for complete combustion). For detailed values of these parameters, Mahinpey presents a complete study on this topic [35].

The last reaction type, the thermal cracking, occurs without the presence of an oxidizing gas. The temperature is usually between the LTO and HTO ranges, but also it is the responsible for coke deposition and considerable amounts of volatile hydrocarbon fractions.

A literature review provides several reaction mechanisms that represents the three stages previously mentioned [6, 36–38]. One of the most used mechanism was proposed by Belgrave as a comprehensive approach to in-situ combustion modeling [9]. The chemical compounds involved in the reactions are modeled as pseudo-components.

Thermal cracking reaction:

$$\text{Maltenes} \longrightarrow 0.372\text{Asphaltenes} \tag{R2}$$

$$\text{Asphaltenes} \longrightarrow 83.223\text{Coke} \tag{R3}$$

$$\text{Asphaltenes} \longrightarrow 37.683\text{Gas} \tag{R4}$$

For LTO R5 and R6 and HTO R7:

$$\text{Maltenes} + 3.431O_2 \longrightarrow 0.4726\text{Asphaltenes} \tag{R5}$$

$$\text{Asphaltenes} + 7.513O_2 \longrightarrow 101.539\text{Coke} \tag{R6}$$

$$\text{Coke} + 1.232O_2 \longrightarrow 0.565H_2O + 0.899CO_2 + 0.1CO \tag{R7}$$

A second mechanism, more complex, detailed and based on SARA fractions, was proposed by Freitag and Verkoczy [39] and has been implemented by Kristensen in his work [13]. This model requires a higher computational cost than the proposed by Belgrave.

Thermal cracking reaction:

$$\text{Arom} \longrightarrow 0.06\text{Asph} + 1.81\text{Lites} \tag{R8}$$

$$\text{Resins} \longrightarrow 0.48H_2O + 0.59\text{Arom} + 0.17\text{Asph} + 0.63\text{Sat} + 0.79\text{Lites} \tag{R9}$$

$$\text{Asph} \longrightarrow 0.55H_2O + 0.18\text{Arom} + 0.54\text{Sat} + 0.19\text{Lites} + 1.43\text{PyrCoke} \tag{R10}$$

For Low temperature oxidation:

$$\text{Resins} + 48.62O_2 \longrightarrow 29.97H_2O + 25.8CO_2 + 1.37\text{OxdResAr} \tag{R11}$$

$$\text{Asph} + 91.66O_2 \longrightarrow 43.87H_2O + 63.5CO_2 + \text{OxdAsph} \tag{R12}$$

$$\text{Arom} + 18.25O_2 \longrightarrow 12.75H_2O + 7.02CO_2 + \text{OxdResAr} \tag{R13}$$

$$\text{Sat} + 18.71O_2 \longrightarrow 14.54H_2O + 10.65CO_2 + \text{OxdSat} \tag{R14}$$

High temperature oxidation:

$$\text{PyrCoke} + 68.3\text{O}_2 \longrightarrow 21.54\text{H}_2\text{O} + 54.89\text{CO}_2 \quad \text{(R15)}$$

$$\text{OxdAsph} + 41.92\text{O}_2 \longrightarrow 15.7\text{H}_2\text{O} + 36.5\text{CO}_2 \quad \text{(R16)}$$

$$\text{OxdResAr} + 26.01\text{O}_2 \longrightarrow 10.72\text{H}_2\text{O} + 24.9\text{CO}_2 \quad \text{(R17)}$$

$$\text{OxdSat} + 12.9\text{O}_2 \longrightarrow 6.22\text{H}_2\text{O} + 10.65\text{CO}_2 \quad \text{(R18)}$$

$$\text{Asph} + 133.58\text{O}_2 \longrightarrow 59.56\text{H}_2\text{O} + 100\text{CO}_2 \quad \text{(R19)}$$

$$\text{Resins} + 84.34\text{O}_2 \longrightarrow 44.68\text{H}_2\text{O} + 60\text{CO}_2 \quad \text{(R20)}$$

$$\text{Arom} + 44.270\text{O}_2 \longrightarrow 23.47\text{H}_2\text{O} + 31.93\text{CO}_2 \quad \text{(R21)}$$

$$\text{Lites} + 18.5\text{O}_2 \longrightarrow 13\text{H}_2\text{O} + 12\text{CO}_2 \quad \text{(R22)}$$

Nesterov provides the kinetic data and stoichiometric coefficients for reactions R8 to R22 [1].

Additionally, some research results from Stanford University developed isoconversional techniques providing model-free methods in order to estimate activation energies [37, 38]. They proved that SARA reaction schemes are not suitable to predict properly the process and also they proposed reaction schemes that match the behavior of the experimental results. The general scheme that most of the studies follow for many kind of oils is:

$$Oil + \text{O}_2 \longrightarrow Coke_1 \quad \text{(R23)}$$

$$Coke_1 + \text{O}_2 \longrightarrow Coke_2 + \text{CO}_2 + \text{CO} + \text{H}_2\text{O} \quad \text{(R24)}$$

$$Coke_2 + \text{O}_2 \longrightarrow \text{CO}_2 + \text{CO} + \text{H}_2\text{O} \quad \text{(R25)}$$

### 1.1.4 Simulation toolboxes

A simulation toolbox is a compilation of mathematical models and solution algorithms to predict the behavior for a defined process under specific conditions and assumptions. The main purpose of these tools is to provide a versatile and useful evaluation of the process.

As mentioned above in the research problem, there are no reports for simulation toolboxes developed specifically for experimental ISC. The closest to such a toolbox would be the use of the various commercial and open-source packages for computational fluid dynamic (CFD) available.

ANSYS (commercial) [40] and OPEN-FOAM (open-source) [41] are powerful tools to simulate the fluid dynamic, but the goal of these software is not the combustion in porous media, due to the high computational cost. STARS is a commercial software, developed by the computer modelling group (CMG) [42], which focuses on reservoir simulation. STARS provides thermal calculations, phase equilibrium based in K-value, chemical reactions and geomechanical models. But the cost of the commercial software is the principal disadvantage to practical use in research applications. Furthermore, none has been particularly designed to model ISC in experimental systems.

On the other hand, CHEMKIN [43] is a robust simulation toolbox that is used for reactor design and experimental evaluation. The most important aspect is the facility to implement modules with different process models for a wide range of applications. Another similar toolbox for reactors design is CANTERA [44], which solves problems such as chemical kinetics, thermodynamics and transport process. But these toolboxes cannot predict the combustion of crude oil in porous media.

## 1.2 Modeling of ISC

The first approaches on in-situ combustion modeling were made by Bailey and Larkin [45], the model includes convection effects unlike the previous studies that they made, in which only heat transfer by conduction was taken into account. The heat balance equation was applied to linear and radial geometries, where the solution was carried out by analytical Laplace transformation for time and finite Fourier transformation for spatial dimensions. Thomas extended the theoretical work to forward combustion in a radial system having a vertical section of infinite thickness [46].

Later, Gottfried [47] presented a better approach with a generalized mathematical model which describes the thermal oil recovery. The model includes: a three-phase fluid flow

under gravity effect, conduction-convection heat transfer, relative permeability and capillary pressure, aqueous phase chance and chemical reaction between oxygen and oil. Further, the system of equations was solved using a finite difference scheme.

As an extension on the previously work, Couch and Rodriguez presented a method to estimate the field fuel consumptions by adjusting laboratory data for the effects of porosity and permeability. The calculations were made for a wide range of crude oil viscosities, and showed that porosity and permeability have a marked effect on fuel consumption depending on the oil viscosity [48].

A two-dimensional, multicomponent with three phases simulator was developed by Farouq Ali [49]. An Arrhenius kinetic model was implemented to represent the complete oxidation. Condensation and vaporization of water were taken into account, but oil was considered undistillable. The solution employs a finite difference discretization scheme, implicit solution in time for pressure and explicit solution for the other variables. The work of Acharya and Somerton [50] was similar to that by Farouq Ali [49] as it represented a vertical cross section of the reservoir, but including the transport of oxygen by diffusion. On the other hand, Crookston et al. [51] developed the first consistent model to represent the ISC process. The model includes condensation and vaporization for water and oil estimated from liquid-vapor equilibrium. But the highlight of the research was the inclusion of pseudocomponents like light and heavy crude oil as precursors of coke, physical properties correlations for temperature changes and also relative permeability data.

Following more detailed numerical methods, Grabowski [52] presented a fully implicit general purpose model (ISCOM) developed by the computer modelling group (CMG) in Calgary. Based on finite difference scheme, ISCOM solved implicit three dimensional systems with Newtonian iteration and a modified form of Gaussian elimination to solve the Jacobian matrix.

Coats [3] describes a comprehensive methodology to develop a rigorous ISC model without simplifications. The model can be used to wet or dry conditions, forward or reverse combustion, and also in one, two or three dimensional geometry. As Grabowski, Coats included a variable number of components, and allowed the components to be distributed in any or all of the four phases (water, oil, gas, and coke).

A novel application of equations of state (EOS) for reservoir simulation was introduced by Young and Stephenson [53]. They proposed a generalized compositional model applied to conventional recoveries with the Redlich-Kwong equation with a careful primary and secondary variable selection. The liquid-vapor equilibrium was modeled as a flash distillation analogy and the solution was proposed as a complex iterative Newtonian method with implicit pressure and explicit saturation (IMPES) technique.

A sensitivity study of the effect of the parameters on results from an in situ combustion simulator was carried out by Anis et al. [54] for one, two and three dimensions. The parameters were block size, dimensionality of the model, number of reactions, activation energy, reaction constant and injection rate. The most sensitive parameters were the block size and dimensionality, which have a strong influence on convection. Even a large block size could inhibit the ignition of the crude oil.

Using the ISCOM simulator Rubin and Buchanan [55] studied hot water injection, steam injection, dry combustion, wet combustion in all dimensions with experimental data validation. Also all the cases applied to Cartesian, radial or curvilinear geometries. Other both experimental and simulation studies were carried out by Fassihi et al. [30] and Onyekonwu et al.[56] The main purpose of their works was to study the effects of important design parameters to determine the best operating conditions. They tested air requirement, combustion front velocity, fuel concentration, oil and rock physical properties and heat losses. Also Fassihi, noted that it is important to study oxygen diffusion, in order to predict if the chemical reactions are kinetically or diffusionally controlled [30, 56].

Based on the methodology of Coats [3], Genrich and Pope [57] developed a one-dimensional model with multiphase flow, to perform efficient calculations of fluid production for dry and wet forward combustion. The model considers four homogenous zones of constant properties, solved by an explicit scheme. Moreover Le Thiez and Lemonnier [58] in the SARIP simulator, studied alternatives to improve numerical stability with an accurate temperature distribution with large gridblock. The contribution of their work was a new formulation using heat-release curve to represent the combustion front.

Belgrave and Moore [9] noted that combustion tubes had not been standardized, due to the radial heat transfer problem reported in previous works. They proposed considerable insights for the heat losses problem such as the higher heat losses results in higher

oxygen requirements, and also combustion tubes dimensions had an important role in heat transfer. Later the same author, Belgrave et al. [10] published a comprehensive approach to in-situ combustion modeling. They presented a consolidation of kinetic models to represent LTO, RTO and pyrolysis reaction of Athabasca bitumen. Also, an application of the reaction model in numerical simulations of adiabatic combustion tubes was included under a RTO test (Ramped Temperature oxidation) without energy balance equation solving due to the controlled temperature.

To predict performance by computing the production of oil, water and gases, Ocalan and Kok developed a one-dimensional forward ISC model with experimental validation. The model is based on the theory of frontal-advance with an analytical description of fractional flow, phase behavior and heat transfer. The results indicate that similar recovery factors are obtained between experiment and simulation, and an interesting result was that the estimated temperature is always lower than the experimental value [59].

As another point of view, Akkutlu and Yortsos [60] presents a novel ISC model with analytical solution. Almost with better computational tools than the previous works of that kind, they studied the self-propagation of the combustion front under both adiabatic and non-adiabatic boundaries. A comprehensive heat transfer treatment was used, which considers overall heat transfer coefficients and infinite large surroundings. As a continuation of their work, Akkutlu and Yortsos [61] studied the propagation of the combustion front, but with the perspective of the heterogeneity effects to understand the viability of the process.

A methodology for efficient integration of stiff kinetics in reactive porous media, was proposed by Kristensen et al. [13]. The aim of the research was the application of Explicit Singly Diagonal Implicit Runge-Kutta (ESDIRK) method in a virtual kinetic cell model. They demonstrated that phase changes cause convergence problems, thus they proposed an algorithm for detection and location of phase changes based on discrete event system theory. Following the study of phase changes in the kinetic cell as well as virtual combustion tube, Kristensen et al. [25] presented a fully compositional model based on an equation of state, where a sensitivity analysis to numerical discretization and combustion front velocity, was carried out.

In order to minimize the impact on the environment, ISC fallows new demands to reduce the emissions of carbon dioxide. Liu [62] presents a model that considers recycling to the reservoir, part of the carbon dioxide produced by ISC. This operation design increases the recovery factor and reduce the emissions to the environment.

As a continuation of Kristensen's works [13, 25], Nesterov et al. [1] included a model based on SARA fractions with a total of fourteen components, which may undergo fifteen chemical reactions. The research results shows that a parameter that affects the process ignition was the activation energy of the oil light fraction.

Recent papers were presented by Youtsos and Mastorakos [63] and Lovett et al. [64] The first one, solved the equations by the method of lines (discretize the spatial derivate and solve an ordinary differential equation for time). The second one, developed an ISC model with adaptive meshing applied to one and two-dimensional lab-scale.

# Chapter 2

# Simulation Toolbox

Figure 2.1 shows the main structure and functionality of the Toolbox. The planning and organization of the subroutines was coded in modular blocks in order to use common calculations between the different reactor models. Input files (default and custom) and thermodynamic data are feeded to the toolbox to be processed. The results and final plots depend on the type of reactor. However, the common outputs for all the models are: moles of species, temperature and numerical information. With the output information is possible to compute saturation, concentration, ratios and others (Post-Processing). Cantera works as an external data provider for the toolbox without using models and special features, only provides properties and reaction rates for gas phase. This chapter is dedicated exclusively to give some detail about modules contained in the Toolbox and the models/correlations that are necessary to calculate physical properties, emphasizing the phase equilibrium.

## 2.1 Cantera

Cantera is a object-oriented software that involves thermodynamic, kinetic and transport phenomena data used in calculations for ideal and non ideal conditions [65].

The software can define different phases with its own thermodynamic, transport and chemical properties in the phase, the inter phase and heterogeneous reactions. It can be also applied to simulate steady and unsteady reacting flows, but in this thesis Cantera

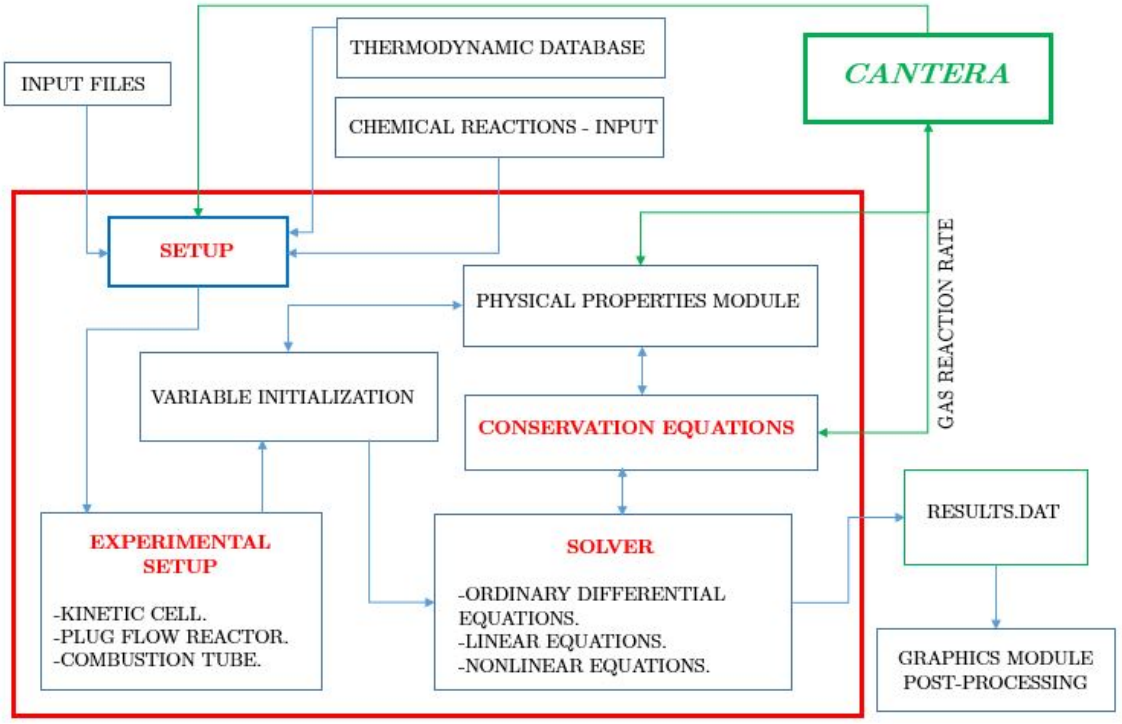


FIGURE 2.1: Schematic structure of the Toolbox.

is only used as a data provider and the models are not interesting for our application as they are not readily applicable to ISC.

Cantera was coupled with the Toolbox through Matlab, using Windows architecture. A custom gas phase database was created from the GRI-Mech 3.0 and enhanced using iodine reactive species (file name FRUN.cti) as later explained. GRI-Mech 3.0 is an optimized mechanism designed to model natural gas combustion, which contains 325 reactions and 53 species [44]. All the rate coefficients, thermochemical data and transport coefficients are available on the Berkeley University webpage (grimech30.dat, thermo30.dat, transport.dat).

## 2.2 Physical properties module

A reaction of ISC involves thermodynamic, kinetic and transport processes, all of them are highly dependent of temperature, pressure and composition. Then different models and data are needed to perform the simulation. The models and the source of the data are explained in this section.

### 2.2.1 Porosity and saturation

Porosity is defined as a measure of the void spaces inside the solid material. In the analyzed system, the space that is not occupied by the solid matter, is filled with gas, oil, water, and coke (see Figure 2.2). Then the void space or volume of pores is defined by the volume that liquid and gas phases occupy, and the filled space is defined by the solid space. The total volume considers the solid matrix, and the pore volume.

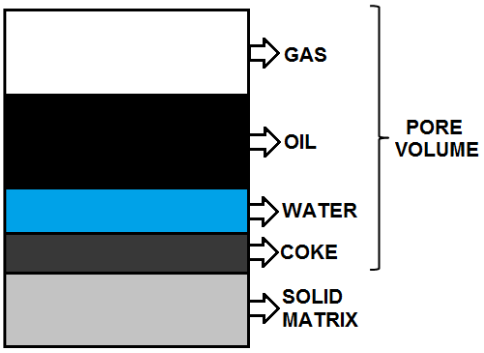


FIGURE 2.2: Schematic composition of the system.

$$\phi = \frac{Pore\ volume}{Total\ volume} \tag{2.1}$$

Then as the pores are filled with the liquid and gas phase, a measure of how much of that phase is in the pore is the saturation, shown in Equation 2.2.

$$S = \frac{Phase\ volume}{Pore\ volume} \tag{2.2}$$

### 2.2.2 Thermodynamic data

Because in the model different pseudo-components were used to represent the oil, gas mixture and solid organic compound, it is necessary to determine the physical properties of these compounds. Table 2.1 shows the properties of the compounds used in the simulations. This kind of data is required on the physical properties correlations and was taken from the CMG user's guide[42]. For oil and coke species, data from Bazargan was enough to complete the inputs [66].

TABLE 2.1: Physico-chemical properties of the pseudo-components used in the model [42, 66].

| Compound | Critical Pressure | Critical Temperature | Molecular weigth | Mass Density |
|---|---|---|---|---|
| | kPa | K | $kg/kmol$ | $(kg/m^3)$ |
| $H_2O$ | 22048 | 647.3 | 18 | 1000 |
| $Oil$ | 1115 | 767.0 | 537.6 | 1008 |
| $N_2$ | 3394 | 126.2 | 28 | IG |
| $O_2$ | 5046 | 154.6 | 32 | IG |
| $CO_2$ | 7376 | 304.2 | 44 | IG |
| $CO$ | 3496 | 132.9 | 28 | IG |
| $Coke_1$ | - | - | 673.04 | 1380 |
| $Coke_2$ | - | - | 179.76 | 1380 |

### 2.2.3 Thermal conductivity

All the phases j have a thermal conductivity associated, $\alpha^j$. The effective thermal conductivity of the porous medium is shown in Equation 2.3 in which a weighted volume average is computed.

$$\alpha = \phi \left( \sum_j \alpha_j S_j \right) + (1 - \phi)\alpha_{rock} \tag{2.3}$$

To have an idea of the order of the values of thermal conductivity of each phase, Table 2.2 shows typical values, it has to be noted that those values can change with the thermodynamic conditions of the system.

In order to make easy calculations, The toolbox can be fixed to work with an overall value of the thermal conductivity (constant without temperature effects): 258.33 $Joule\, m^{-1}\, min^{-1}\, K^{-1}$

### 2.2.4 Internal energy and enthalpy

The phase enthalpy is computed from the ideal gas heat capacity of the pseudo-components and the vaporization enthalpy. The heat capacity is also highly temperature dependent,

TABLE 2.2: Tipical values for thermal conductivity.

| Phase | Thermal conductivity $\left[\frac{J}{m \cdot min \cdot K}\right]$ |
|---|---|
| Water | 37.15 |
| Oil | 7.98 |
| Gas | 1.25 |
| Coke | 312.50 |
| Rock | 141.60 |

and as a consequence it has to be calculated every time that conditions change, the value for the rock matrix is 1.20572 $Joule\, cm^{-3}\, K^{-1}$ and for the other components is computed with Equation 2.4. The units of the equation are given in $Joule\, mol^{-1}\, K^{-1}$. Parameters a,b, c and d are shown in Table 2.3.

$$Cp = a + bT + cT^2 + dT^3 \tag{2.4}$$

TABLE 2.3: Heat capacity and vaporization enthalpy parameters [42]. See the text for an explanation of the use of the different terms.

| Phase | $a$ | $b$ | $c$ | $d$ | $hv^1$ | $hv^2$ |
|---|---|---|---|---|---|---|
| $Coke_1$ | 17.00 | 0 | 0 | 0 | 0 | 0 |
| $Coke_2$ | 17.00 | 0 | 0 | 0 | 0 | 0 |
| $Oil$ | 1138.80 | 0 | 0 | 0 | 8569 | 0.38 |
| $Water$ | 32.24 | $1.924 \times 10^{-3}$ | $1.055 \times 10^{-5}$ | $-3.596 \times 10^{-9}$ | 4820 | 0.38 |
| $N_2$ | 31.15 | $-1.357 \times 10^{-2}$ | $2.680 \times 10^{-5}$ | $-1.168 \times 10^{-8}$ | 0 | 0 |
| $O_2$ | 28.11 | $-3.680 \times 10^{-6}$ | $1.746 \times 10^{-5}$ | $-1.065 \times 10^{-8}$ | 0 | 0 |
| $CO$ | 30.87 | $-1.285 \times 10^{-2}$ | $2.789 \times 10^{-5}$ | $-1.272 \times 10^{-8}$ | 0 | 0 |
| $CO_2$ | 19.80 | $7.344 \times 10^{-2}$ | $5.602 \times 10^{-5}$ | $1.715 \times 10^{-8}$ | 0 | 0 |

The enthalpy of the ideal gas pseudo-components is calculated from Equation 2.5, the vaporization enthalpy is calculated with the correlation presented in Equation 2.6 (only for $T_i^{crit}$ >T). For the case of ideal gas, the enthalpy of the phase is calculated with

Equation 2.7, finally the oil and water phase enthalpies are calculated with Equations 2.8 and 2.9.

$$h_i^g = \int_{T_{ref}}^{T} Cp_i(T)dT \tag{2.5}$$

$$h_i^{vap} = hv_i^1(T_i^{crit} - T)^{hv_i^2} \tag{2.6}$$

$$h_i^g = \sum_i y_i h_i^g \tag{2.7}$$

$$h_i^o = \sum x_i^o \left(h_i^g - hv_i^{vap}\right) \tag{2.8}$$

$$h^w = (h_w^g - hv_w^{vap}) \tag{2.9}$$

The internal energy for phase j is calculated by Equation 2.10.

$$U^j = h^j - \frac{P}{\rho} \tag{2.10}$$

where P is the pressure, $\rho$ the density and $x_i$ is the molar fraction of the component i.

### 2.2.5 Relative permeability

Permeability is a measure of how easy a fluid can pass through a solid. Now, when the system has different fluids, each of them reaches different velocities, then the relative permeability relates the change in flow of the fluid due to the presence of different fluids. It depends on the porosity and geometry of the pore, wettability, fluid distribution and fluid saturation.

A model that considers water as the wetting phase is shown in Equation 2.11, in which the relative permeabilities of the wetting and nonwetting phases ($k_{rw}$, $k_{rg}$), the relative permeability to oil in the oil-water system ($k_{row}$) and the relative permeability to oil in the oil-gas system ($k_{rog}$) are obtained by experiments, and the data are shown in Table 2.4 where $SI = S_W + S_O$.

$$k_{ro} = (k_{row} + k_{rw})(k_{rog} + k_{rg}) - (k_{rw} + k_{rg}) \tag{2.11}$$

TABLE 2.4: Permeabilities and calculation of relative permeabilities [66].

| $\%S_W$ | $k_{rw}$ | $k_{row}$ | SI | $k_{rg}$ | $k_{rog}$ |
|---|---|---|---|---|---|
| 0 | 0 | 1 | 0 | 0.8975 | 0 |
| 0.068 | 0 | 1 | 0.068 | 0.8975 | 0 |
| 0.15 | 0.0077 | 0.8229 | 0.1368 | 0.75 | $1 \times 10^{-3}$ |
| 0.2 | 0.02 | 0.7232 | 0.2 | 0.6233 | 0.0077 |
| 0.218 | 0.0259 | 0.6889 | 0.25 | 0.5429 | 0.02 |
| 0.25 | 0.0381 | 0.63 | 0.268 | 0.5154 | 0.0259 |
| 0.3 | 0.0619 | 0.5432 | 0.3 | 0.4681 | 0.0381 |
| 0.35 | 0.0915 | 0.4629 | 0.35 | 0.3989 | 0.0619 |
| 0.4 | 0.1268 | 0.3889 | 0.4 | 0.3352 | 0.0915 |
| 0.45 | 0.1679 | 0.3214 | 0.45 | 0.277 | 0.1268 |
| 0.5 | 0.2148 | 0.2604 | 0.5 | 0.2244 | 0.1679 |
| 0.55 | 0.2674 | 0.2057 | 0.55 | 0.1773 | 0.2148 |
| 0.6 | 0.3258 | 0.1575 | 0.6 | 0.1357 | 0.2674 |
| 0.65 | 0.3899 | 0.1157 | 0.65 | 0.0997 | 0.3258 |
| 0.7 | 0.4598 | 0.0804 | 0.7 | 0.0693 | 0.3899 |
| 0.75 | 0.5354 | 0.0514 | 0.75 | 0.0443 | 0.4598 |
| 0.8 | 0.6168 | 0.0289 | 0.8 | 0.0249 | 0.5354 |
| 0.85 | 0.704 | 0.0129 | 0.85 | 0.0111 | 0.6168 |
| 0.9 | 0.7969 | 0.0032 | 0.9 | 0.0028 | 0.704 |
| 1 | 0.8956 | 0 | 1 | 0 | 0.8956 |

### 2.2.6 Viscosity

The viscosity is defined as the resistance to flow. As flow is related with molecular movement, the viscosity is highly dependent of the temperature, and as a consequence some models have been developed in order to calculate the viscosity at a certain temperaure, Equation 2.12 show a correlation proposed by Belgrave et al. [10] for component i in the oil and water phases. The model consider two parameters A and B, which are determined by experiments.

$$\mu_i = Ae^{\left(\frac{B}{T}\right)} \tag{2.12}$$

TABLE 2.5: Viscosity parameters for the components in the oil phase and for the water phase [10]

| Compound | A ($cp$) | B ($^oC$) |
|---|---|---|
| Oil | $4.89 \times 10^{-25}$ | 33147 |
| Water | 0.00752 | 1384.86 |

For the case of gases, the viscosity is calculated using the Sutherland's formula shown in Equation 2.13 [67]. The equation has two main parameters a and b, which are calculated from Sutherland's constant and the reference temperature, the values of the Sutherland's constant, the reference temperature and viscosity for the gases are given in Table 2.6.

$$\mu = \mu_0 \left(\frac{a}{b}\right) \left(\frac{T}{T_0}\right)^{(3/2)} \tag{2.13}$$

$$a = 0.555T_0 + C \tag{2.14}$$

$$b = 0.555T + C \tag{2.15}$$

TABLE 2.6: Sutherland's constant, reference temperature and viscosityfor gases viscosity calculation [67]

| Gas | Sutherland's constant, C | $T_o(^oR)$ | $\mu_0$ (centipoise) |
|---|---|---|---|
| Standard air | 120 | 524.07 | 0.01827 |
| $CO_2$ | 240 | 527.67 | 0.01480 |
| CO | 118 | 518.67 | 0.01720 |
| $H_2$ | 72 | 528.93 | 0.00876 |
| $N_2$ | 111 | 540.99 | 0.01781 |
| $O_2$ | 127 | 526.05 | 0.02018 |

Aditionally, when the correlation coefficients are not available for the oil, users can make a viscosity table as an input file in the form of Table 2.7.

TABLE 2.7: Oil viscosity table [66].

| Temperature °C | $\mu_{oil}$ Centipoise | Temperature °C | $\mu_{oil}$ Centipoise |
|---|---|---|---|
| 5 | 1636262 | 325 | 0.75 |
| 15 | 229374 | 350 | 0.60 |
| 25 | 54485.9 | 375 | 0.50 |
| 30 | 30000 | 400 | 0.47 |
| 48 | 10600 | 425 | 0.41 |
| 65 | 3000 | 450 | 0.36 |
| 100 | 290 | 475 | 0.315 |
| 150 | 32 | 500 | 0.28 |
| 200 | 7.5 | 525 | 0.25 |
| 250 | 2.7 | 550 | 0.22 |
| 300 | 1.0 | 2000 | 0.12 |

### 2.2.7 Coefficient of thermal expansion and compressibility

The concept of this coefficient gives an idea of the compressible properties of substances and it can be seen as the reciprocal of the elasticity modulus of the bulk, in which gases are more compressible than the others phases. Isothermal gas compressibility is defined by Equation 2.16. From the real gases law, Equations 2.17, 2.18 and 2.19, an expression on terms of z and p is derived and Equation 2.20 is obtained.

$$c_j = -\frac{1}{V_j}\left(\frac{\partial V_j}{\partial p}\right)_T \tag{2.16}$$

$$\left(\frac{\partial V_j}{\partial p}\right)_T = \frac{nRT}{p}\left(\frac{\partial z}{\partial p}\right)_T - \frac{znRT}{p^2} = \left(\frac{znRT}{p}\right)\frac{1}{z}\frac{dz}{dp} - \left(\frac{znRT}{p}\right)\frac{1}{p}... \tag{2.17}$$

$$\frac{1}{V_j} = \frac{p}{znRT} \tag{2.18}$$

$$\frac{1}{V_j}\left(\frac{\partial V_j}{\partial p}\right)_T = \frac{1}{z}\frac{dz}{dp} - \frac{1}{p} \tag{2.19}$$

$$c_j = \frac{1}{p} - \frac{1}{p}\frac{dz}{dp} \tag{2.20}$$

## 2.3 Phase Equilibrium

As previously mentioned, the combustion process in porous media is complex as it involves important chemical and physical changes. Without neglecting the importance of the phases in chemical reactions, we focus our interest on the difference between liquid and vapor, in terms of mass and energy transport due to the wide gap between physical properties.

The distribution of components in the vapor and liquid phases, is usually assumed to be in equilibrium state. This is physically reasonable because the mass transfer occurs much faster than the fluid flow.

A multicomponent system is in themodynamic equilibrium, when the mixture fugacities $\hat{f}$, for each component between phases are equal. Cosider the system with oil, water and gas presented in Figure 2.3, where oil and water are inmiscible in the liquid phase, the vapor-liquid equilibrium VLE is represented as follows:

$$\hat{f}_{i,o}^{G} = \hat{f}_{i,o}^{L} \tag{2.21}$$

$$\hat{f}_{i,w}^{G} = \hat{f}_{i,w}^{L} \tag{2.22}$$

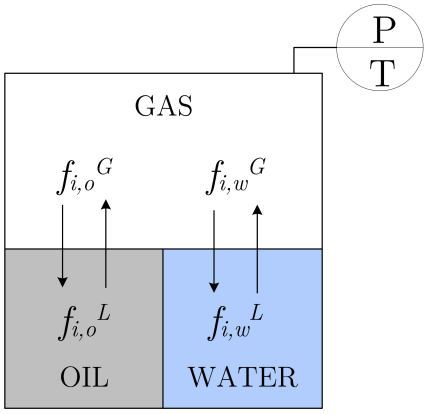


FIGURE 2.3: Phase equilibrium for the system Oil/Water/Gas.

Aqueous components exist in both gas and water phases, while oleic components exist in the oil and gas phases. In this thesis, we only take into account the vapor-liquid equilibrium VLE.

The components fugacities in the gas phase are calculated as follows:

$$\hat{f}_{i,o}^{G} = \hat{\phi}_i y_i P \tag{2.23}$$

where $\hat{\phi}$ is the fugacity coefficient, $y_i$ the gas phase mole fraction, and P the pressure. For the liquid fugacities, we have this expression:

$$\hat{f}_{i,o}^{L} = a_i x_i \phi_i^{sat} P_i^{sat} e^{\frac{V_i(P-P_i^{sat})}{RT}} \tag{2.24}$$

where $a_i$ is the activity coefficient, $x_i$ the liquid molar fraction, $V_i$ is the molar volume and $P_i^{sat}$ is the saturation pressure. The exponential part of the equation is a correction for higher pressures, usually called Poynting factor. If we set the equilibrium state, the phases interaction are given by:

$$K_i = \frac{y_i}{x_i} = \frac{a_i \phi_i^{sat} P_i^{sat} e^{\frac{V_i(P-P_i^{sat})}{RT}}}{\phi_i P} \tag{2.25}$$

Which is the most general expression for the K- value, also as a function of pressure, temperature and composition. For ideal liquid phase, the activity coefficient is equal to the unit, and hence the K-value is only function of pressure and temperature. Also, if the gas phase is considered as ideal state (fugacity coefficient equals to the unit), the equilibrium would follows Raoul's law, where the molar fraction ratio is a function of partial and saturation pressures.

The rigorous calculations of the phase equilibrium are made through cubic equations of state (EOS), but also it is possible to perform estimations of the K-value using correlations. The most common correlation, used in commercial simulators such as STARS, is presented in Equation 2.26.

$$K_i = \frac{y_i}{x_i} = \left(\frac{Kv1}{P} + Kv2 \times P + Kv3\right) e^{\left(\frac{Kv4}{T-Kv5}\right)} \tag{2.26}$$

where $Kv1$, $Kv2$, $Kv3$, $Kv4$ and $Kv5$ are constants that can be found in STARS user's guide for various industry compounds [42].

### 2.3.1 Flash calculations

To have a clear idea of the solution strategy for flash calculations, let's consider the overall mass balance for the water without any aqueous components ($x_w = 1$):

$$m_i^{total} = \sum_j^{np} m_{ij} \tag{2.27}$$

$$\frac{\partial}{\partial t}\left(m_w^{total}\right) = \frac{\partial}{\partial t}\left(m_w^V + m_w^L\right) = V_{total}\frac{\partial}{\partial t}\left(\rho_g S_g y_w + \rho_w S_w\right) \tag{2.28}$$

Thus, for each time step and iteration of the ODE solver, the program has to estimate the phase distribution by splitting the total mass (oil, water and gas) to vapour and liquid streams. Figure 2.4 shows a comprehensive scheme of the flash process.

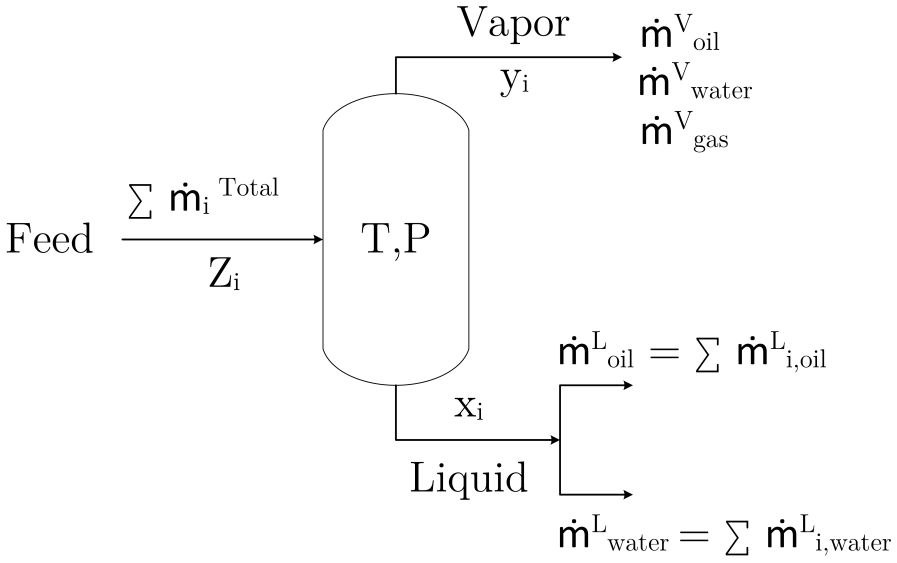


FIGURE 2.4: Flash distillation.

The flash calculation assumes that the total mass of oil, water and gas is splitted from the same feed stream. This approach allows to include the interaction, between gas phase and liquids. Thus, the overall molar fraction in the feed stream can be calculated as:

$$Z_i = \frac{m_i^{total}}{m_w^{total} + m_o^{total} + m_g^{total}} \tag{2.29}$$

Once the K-value has been estimated with EOS or correlations, the phase distribution is calculated from flash distillation algorithms, such Rachford and Rice [23], performing Newton iterations. In terms of computational efficiency and convergence, we use a modified Rachford and Rice algorithm, where the objective function and molar fractions are calculated from:

$$y_i = \frac{Z_i K_i}{1 + \Psi(K_i - 1)} \tag{2.30}$$

$$x_i = \frac{Z_i}{1 + \Psi(K_i - 1)} \tag{2.31}$$

$$\Psi = \frac{Vapor}{Feed} \tag{2.32}$$

$$F(\Psi) = \sum_{i=1}^{nc} y_i - \sum_{i=1}^{nc} x_i = \sum_{i=1}^{nc} \frac{Z_i (K_i - 1)}{1 + \Psi (K_i - 1)} = 0 \tag{2.33}$$

where $\Psi$ is the vapour fraction, and it is the only variable necessary to solve the overall mass balance. Figure 2.5 shows the algorithm that must be followed to find the vapour fraction.

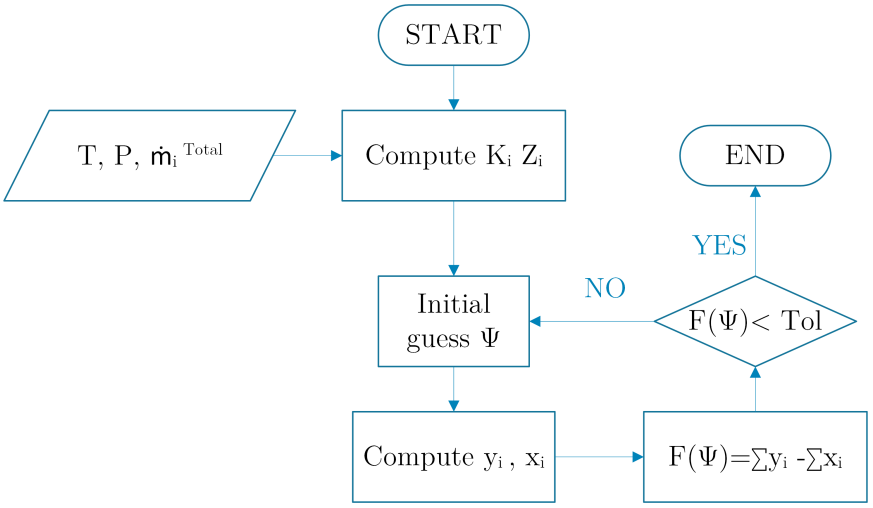


FIGURE 2.5: Rachford & Rice algorithm.

The modified Rachford and Rice Objective function has been proven to be a monotonically decreasing function, and therefore guarantees convergence in Newton-Raphson

iterations. Once the calculations for components mass on each phase are carried out, the physical properties, saturations and enthalpies can be estimated.

As a final remark of this section, the result of the flash calculation are the molar fractions and the mass of each component in the gas and liquid phases. However, if we look at Figure 2.4, The liquid phase contains water and oil, so it is necessary to separate both phases and recalculate the liquid mole fractions for oleic and aqueous components.

## 2.4 Solver module

The software developments that solve the mathematical models were written in Matlab language under Windows architecture [68]. The routine ode15s was implemented to solve ODEs and routine fsolve was used to solve newton iterations for phase equilibrium algorithm. Additionally, Matlab offers a great and powerful user interfase with graphical debugging.

### 2.4.1 Ordinary differential equations (ODEs)

Regardless of the type of reactor, all the toolbox was codified to generate and solve coupled systems of ordinary differential equations (ODEs) denoted by $\dot{X}$, where $X$ is the vector of variables with dimensions $nc + 2$.

$$\dot{X} = \begin{bmatrix} \frac{\partial N_1}{\partial t} \\ \vdots \\ \frac{\partial N_i}{\partial t} \\ \frac{\partial T}{\partial t} \\ \frac{\partial P}{\partial t} \end{bmatrix} \tag{2.34}$$

$$X = \begin{bmatrix} N_1 \\ \vdots \\ N_i \\ T \\ P \end{bmatrix} \tag{2.35}$$

The independent variable is time and is necessary to set the initial value for all the dependent variables $X_0$ on a time interval $t_0 \leq t \leq t_f$.

$$X(t_0) = X_0 \tag{2.36}$$

Particularly, the in situ combustion process is characterized for the stiffness behavior which means that most of the common ODE solver will not get a numerically stable solution. So various numerical strategies should be implemented to avoid this kind of problem. In this work, a stiff ODE solver was implemented from the Matlab library: ode15s which is based on efficient numerical differentiation formulas (NDFs).

This kind of solver does not allow a fixed time step sizing, only interval restrictions and other controls, resulting in a challenging problem when numerical instabilities appear in the simulation. In Chapter 5 we mention some tips to handle this kind of problems.

A paper from Shampine and Reichelt can be reviewed for further information about the matlab libraries to solve ODEs [69].

# Chapter 3

# Toolbox: Kinetic Cell

Kinetic cells are one of the most important equipment for ISC process. With specific experimental configurations, low oil saturation and accurate temperature control, it is possible to exclude the fluid and heat transfer dynamics to study chemical kinetics, ignition temperatures and phase behaviour.

Figure 3.1 shows a normal experiment in a kinetic cell consist on a packed tube with a mixture of crude oil, sand, clay and water. Under a programmed heating rate with an external heat source, air is injected at a constant flow rate to burn the oil sample, where the produced gases and residual solid components are recovered for the analysis. If the operation is carried out with an inert gas such as nitrogen, pyrolysis reactions can be also studied.

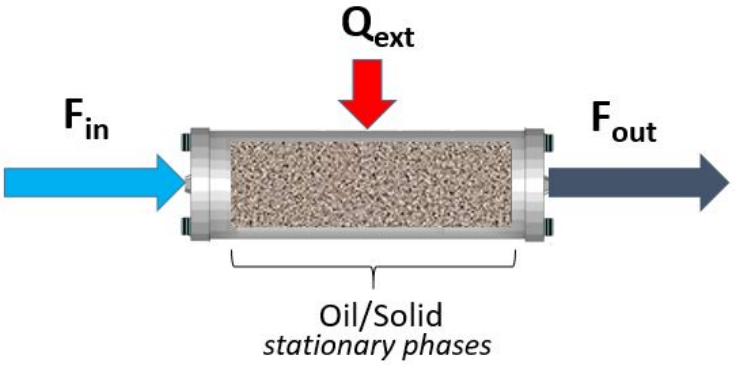


FIGURE 3.1: Schematic diagram for Kinetic cell experiment.

The Toolbox was designed to work with flexible operating conditions, when the common experiments Ramped Temperature Oxidation (RTO) and isothermal oxidation are also included. With simple changes in the input data, it is possible to simulate Thermogravimetric analysis (TGA) under oxidative or cracking conditions.

In the case of kinetic cells with controlled furnace, it was necessary to include energy transfer coupled with set point control, because the exothermic reactions occur faster than the controller action. If this effect is not taken into account, the disturbed temperature profile can cause errors in the kinetic data prediction, as mentioned in [70]. To simulate a varying temperature coupled with set point control with commercial thermal simulators such as STARS [42] is not a simple ordeal, because these softwares are designed for reservoir simulation and not for the analysis of experimental data. These difficulties have been mentioned before, see e.g. [66].

The effect of the heat of reaction on the heating rate can be neglected using an induction reactor (see Figure 3.2) [71]. The action of the controller is almost instantaneous leading to a homogeneous temperature condition according to the heating rate. Also the induction reactor can operate with heating rates over 3°C/min, which is the usual operating condition in furnace kinetic cells. The capacity of the induction reactor to operate in overheating ranges, provides more consistent data, because in the real combustion process the temperature profiles shows heating rates in the reaction zone between 15 and 30°C/min.

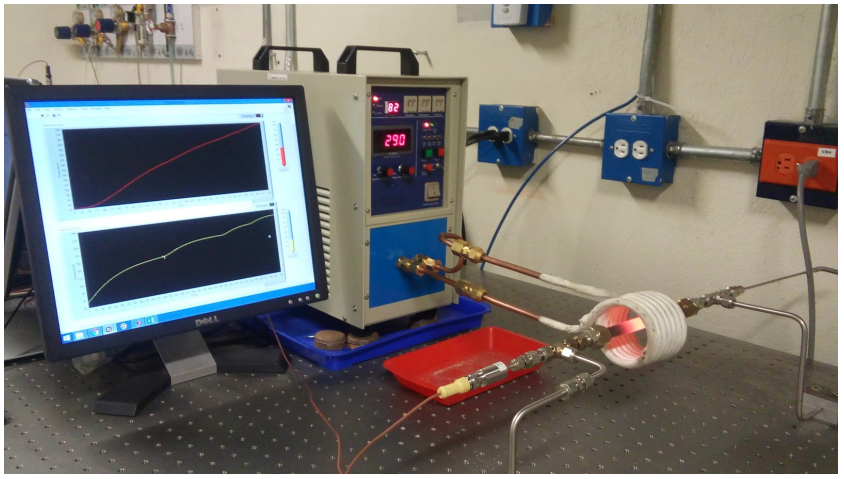

FIGURE 3.2: Kinetic cell heated by induction. FRUN research group, Colombia [72].

Kinetic cell models have been studied for decades. Previous works used numerical simulation as a tool to understand and predict the oil reactivity in porous media. A simplified kinetic cell model to match the experimental data with similar reaction schemes such as that by Dechelette [73] was developed performing simulations with kinetic data from isoconversional analysis [37, 38, 66]. The concept of virtual kinetic cell (VKC) was introduced by Kristensen [74], who proposed robust integration methods such as ESDIRK (implicit one-step Explicit Singly Diagonal Implicit Runge-Kutta) to solve compositional stiff kinetics [13]. The VKC model was improved to include phase equilibrium and then Priyanka [75] continued the work simulating a reaction mechanism based on SARA fractions.

The kinetic cell model in this work was developed with the chemical engineering perspective, based on mole balance. The referred literature could be confusing sometimes, due to the use of concentrations instead of mole or mass of the component, because some authors base the calculations on the porous volume and others on rock matrix volume. The use of overall quantity variables based on mole or mass, leads to a comprehensive sense of the conservation equations, and also a very straightforward implementation and understanding of the code.

## 3.1 Governing equations

The kinetic cell is modeled as a zero-dimensional Semi-Batch reactor (adapted to porous media and multiphase reactor), where only gas flows through the reactor and oil/solid phases are considered stationary. A schematic of the cell chamber is shown in Figure 3.1.

Due to the involved timescales, all the processes inside the kinetic cell are considered in thermodynamic equilibrium, without temperature and pressure gradients. Oil and water are immiscible, and also molecular diffusion is not taken into account, because Peclet numbers for typical reservoir flows of interest are often large enough that the effects of diffusion can be neglected [13].

The general mole balance of species $i$ in the kinetic cell can be expressed as follows:

$$\frac{dN_i}{dt} = \sum_j F_{i,j}^{in} - \sum_j F_{i,j}^{out} + \sum_r \Lambda^{i,r}\gamma^r \quad [=] \quad \frac{mol}{time} \tag{3.1}$$

where $N_i$ represents the amount of moles in the porous medium of species $i$. $F_{i,j}^{in}$ and $F_{i,j}^{out}$ are the inlet and oulet molar flow rates for species $i$ and phase $j$. Finally, $\gamma^r$ and $\Lambda^{i,r}$ are the reaction rate and the stoichiometric coefficient for species $i$ and reaction $r$.

For oil and solid phases, there is not inlet and oulet flow. Equation 3.1 can be simplified as follows:

$$\frac{dN_i}{dt} = \sum_r \Lambda^{i,r}\gamma^j \quad [=] \quad \frac{mol}{time} \tag{3.2}$$

The implementation of volumetric flow, to estimate the outlet flow may cause mass conservation problems, due to the change in moles in the gas phase. Due to the high mobility of the gas in a unconsolidated sand, a good approximation to calculate the outlet flow is to assume that there is not gas accumulation in the system. So the outlet molar flow can be estimated from:

$$F_{i,gas}^{out} = F_{i,gas}^{in} + \sum_r \Lambda^{i,r}\gamma^r \tag{3.3}$$

For RTO experiments, the heating rate can be affected by reaction heat. To perform a simulation which can capture heating effects, it is necessary to include a energy balance, such as that in Equation 3.4, to predict the temperature variation.

$$\sum_i N_i Cp_i \frac{dT}{dt} = -\sum_i F_{i,gas}^{out} Cp_i (T - T^{in}) + \sum_r \Lambda^{i,r}\gamma^r \triangle H_{reac}^r + Q^{ext} \tag{3.4}$$

where $Cp_i$ is the heat capacity of species $i$, $Q^{ext}$ the heat flux from the furnace and $\triangle H_{reac}^r$ the reaction enthalpy.

$$Q^{ext} = UV_{cell}(T^{setpoint} - T) \tag{3.5}$$

$$T^{setpoint} = T^{initial} + \theta t \tag{3.6}$$

The external heat flux is a function of the global heat transfer coefficient $U$, the cell volume $V_{cell}$ and the furnace control set point, which is calculated from the heating rate $\theta$.

## 3.2 Model validation

As was mentioned before, several studies have been conducted to understand kinetic cells such as [6, 8, 37, 38, 66, 73, 76]. These studies present experimental results related to the measurement of outlet gases and residual stationary components (oil and solids). Despite the existence of these multiple studies, one of the difficulties to simulate the ISC process in kinetic cells is to find reliable experimental data in the literature. Most of the kinetic data and physical properties, required in the simulations, are not given in detail. Fortunately, to verify the consistency of the numerical solution in the Simulation Toolbox, the results and input data from Bazargan's thesis were enough to simulate the same experimental setup [66].

TABLE 3.1: Simulation input data for model validation [66].

| Parameter | Value |
|---|---|
| Pressure | 689.480 kPa |
| Inlet air flow (atmospheric) | 0.4172 mol/min |
| Reactor Volume (4 cm packed) | $3.02 \times 10^{-5} m^3$ |
| Oil Molecular weight | 537.6 g/mol |
| Initial temperature | 298.15 K |
| Initial Oil in place | 0.0037 mol |

In [66], the authors predicted kinetics for RTO experiments, based on the analysis of the oxygen consumption and conversion. The consumption percent is calculated as follows from the difference of the molar fractions,$yO_2$, between inlet (usually 0.21 oxygen molfrac.) and outlet:

$$O_2 consumption = \left( yO_2^{inlet} - yO_2^{outlet} \right) \times 100 \tag{3.7}$$

TABLE 3.2: Kinetic data used for kinetic cell validation [66].

| Reaction | Frecuency factor $\left[\frac{1}{min \times kPa}\right]$ | Activation energy $\left[\frac{J}{mol}\right]$ |
|---|---|---|
| R26 | 207.197 | 63560 |
| R27 | 552.525 | 87525 |
| R28 | 690.656 | 97575 |

The kinetic cell has a diameter of 3.1 cm and length of 12 cm, but only 4 cm were saturated with 2 gr of crude oil and then filled with nitrogen in order to guarantee an inert medium. The experiment was carried out with an injection of atmospheric air flow. A summary of operating and initial conditions is presented in Table 3.1.

To obtain the oxygen consumption profile for a heating rate of 3°C/min, we perform the simulations with the kinetic data presented in Table 3.2 and the reaction mechanism from R26 to R28.

$$Oil + 4.24O_2 \longrightarrow 0.3659Coke_1 \tag{R26}$$

$$Coke_1 + 33.8O_2 \longrightarrow 6.8642Coke_2 + 19.77CO_2 + 26.06CO \tag{R27}$$

$$Coke_2 + 12.29O_2 \longrightarrow 9.21CO_2 + 6.16CO \tag{R28}$$

We present the total moles of the components, and also the reaction rate is calculated multiplying the reaction rate coefficient by the moles of oil or coke in each time step. With the chemical engineering approach that we use in the Toolbox models and the presented data is enough to get the oxygen consumption.

Figure 3.3, shows the results of the simulation compared with the data taken from the thesis of Bazargan [66]. There is a clear match between the two profiles, for LTO reactions (under 400°C) and for HTO reactions (over 400°C). This kind of consumption profile is very useful for isoconversional analysis. Also, it is possible to calculate the conversion as a function of time and temperature, with just performing numerical integration over the profile.

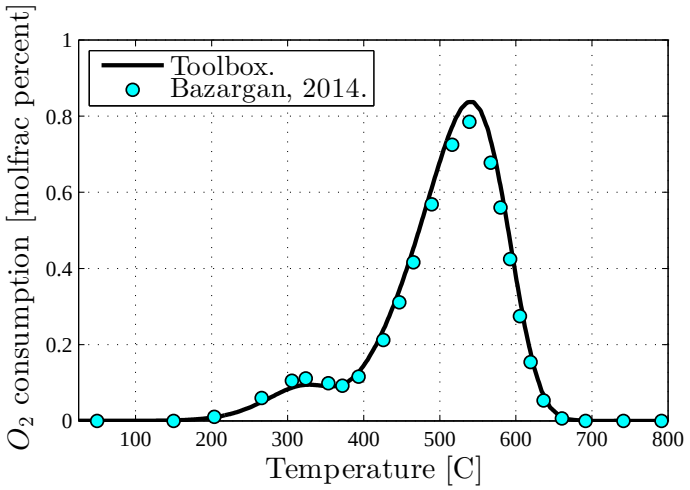


FIGURE 3.3: Oxygen consumption profile. Comparison between Toolbox (Solid line) and Bazargan's results (filled circles). Heating rate of 3°C/min [66].

## 3.3 Toolbox Applications

As we mentioned before, the Toolbox is versatile and can be used for different operating conditions. Once we show that the developed model for the kinetic cell is able to match the same profiles from the ISC literature, we proceed to study the application of the Toolbox to three different problems related to ISC: RTO and isothermal experiments, combustion dynamics with gas phase reactions and single phase flow and halogen injection for the analysis of CO oxidation. In some of these applications sensitivity analyses were undertaken to understand the importance of the most important experiment variables. All the Toolbox applications in this chapter are based on the physical properties in Chapter 2 and the parameters in Table 3.3. Furthermore, due to small amounts in moles of some species involved on gas phase reactions, the numerical tolerances were fixed on $10^{-10}$. Operating conditions may vary. However, in that case, changes are presented in each section.

### 3.3.1 RTO experiments

RTO experiments are widely used to understand the oil reactivity in a similar environment as the real process. The heating rates can change drastically in the reaction zone, even taking values about 30°C/min [66]. RTO experiments and isothermal analysis, can

TABLE 3.3: Kinetic cell parameters. FRUN research group.

| Parameter | Value |
|---|---|
| Diameter | $0.0127m$ |
| Length | $0.12m$ |
| Reactor Volume | $1.5201 \times 10^{-5} m^3$ |
| Porosity | 0.378 |
| Initial temperature | $298.15K$ |
| Pressure (constant) | $101.13kPa$ |

be used to infer kinetic parameters which are important to predict and upscale the process. It is, therefore, of interest to understand the response of the Toolbox to different heating ramps. Such simulations, carried out using the kinetic parameters from Table 3.2, are presented below.

Simulation conditions (RUN-1): Gas volumetric injection rate of 2L(SATP)/min with a composition of y$O_2$: 0.21, y$H_2O$: 0.001 and yN2: 0.789. Heating rates of 2, 10, 30, 50°C/min. The initial gas saturation was fixed as 0.8, while oil saturation as 0.2. The kinetic cell initial pressure was 101.13 kPa and remained constant.

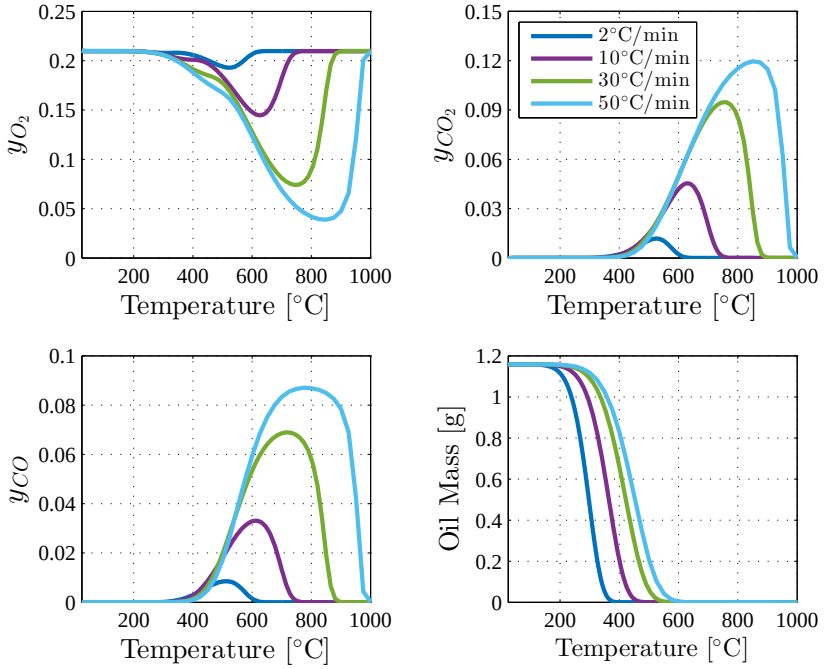


FIGURE 3.4: Kinetic cell profiles versus temperature for different heating rates. Oil mass, $y_{O_2}$, $y_{CO_2}$ and $y_{CO}$ molar fractions.

Figure 3.4 shows the results for the RTO experiments. The duration of each experiment is totally different, so for better comparison between the experiments, all the profiles were plotted versus temperature. For large heating rates, the decrease in the oxygen molar fraction is more important than lower rates. But also, the total oxygen consumption, calculated from the numerical integration of the profile, is the same for all the heating rates. In this case, the series of fuel formation reactions (sequence of $Oil \rightarrow Coke_1 \rightarrow Coke_2$) demand that all the fuel will be burned, even if the process of coke formation takes few minutes or hours. Therefore, the oxygen consumed will be the stoichiometric from the chemical coke oxidation reactions. While the independence of oxygen consumption on heating rate, agrees with the particular reaction mechanism from R26 to R28, that may not be the case for ISC experiments nor for other gases. Even if we do not consider thermal cracking and also reactions competing at low oxygen concentrations, gas phase reactions, such as carbon monoxide oxidation, can change the profiles as described below.

### 3.3.2 Combustion dynamics with gas phase reactions

As mentioned above, gas phase reactions could affect the gas concentration profiles. This phenomena can be captured by coupling the Toolbox and Cantera, which can easily add gas-phase carbon monoxide reactions with kinetic data from GRI-Mech 3.0 to a typical ISC mechanism.

To evaluate possible differences that any extent of gas-phase CO oxidation may cause on typical ISC simulations that only consider heterogeneous chemistry, and to illustrate the simplicity of these calculations in the toolbox, a combined RTO-Isothermal thought experiment was designed to oxidize both oil and carbon monoxide. Additionally, another experiment was conducted only under isothermal conditions.

Simulation conditions (RUN-2): Volumetric injection rate of 300 mL(SATD)/min with a composition of y$O_2$ : 0.21, y$H_2O$: 0.001 and y$N_2$: 0.789. Heating rate of 30°C/min until 800°C, then isothermal operation at 800°C. The initial gas saturation was fixed at 0.9, while oil saturation at 0.1.

Note the presence of water in the oxidizer stream. That is due to the importance of the hydroxyl radical ($OH^*$) on carbon monoxide oxidation. The analysis, in Figure 3.5,

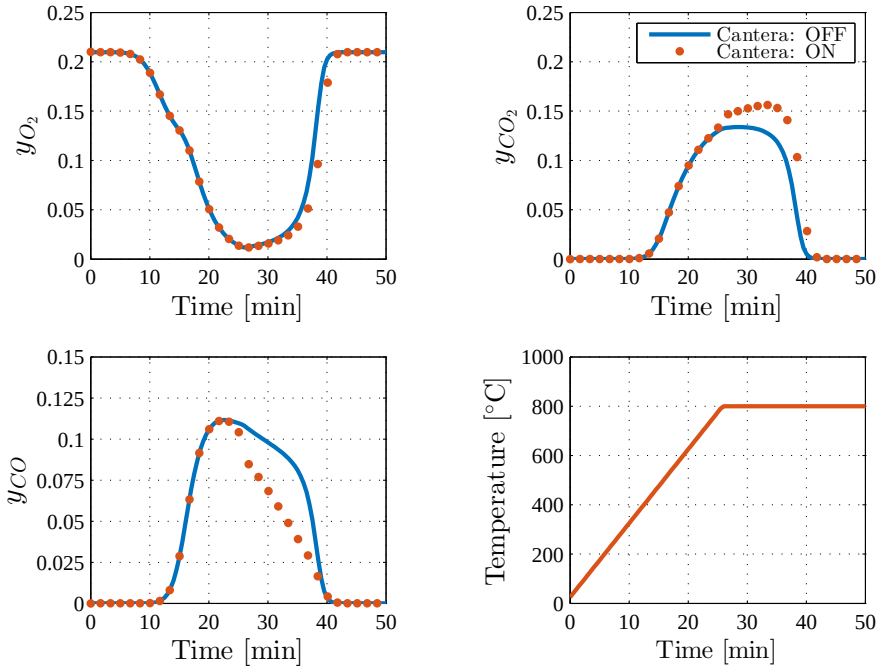


FIGURE 3.5: In situ combustion profiles for a combined RTO-isothermal experiment. Gas phase reactions activated and deactivated.

of the simulation for RUN-2, compares the results when considering or not gas phase reactions. At temperatures higher than 700°C CO oxidation becomes important, as CO concentration is less than the expected in a regular combustion without Cantera reactions, and also carbon dioxide shows an increase because is the final product in the CO oxidation. The oxygen profile is slightly different compared to the normal oxygen profile, although in Figure 3.6, it is possible to identify the oxidation of $Coke_2$ at the same time that CO oxidation (between 22 and 40 minutes). So the coke combustion requires more oxygen than carbon monoxide.

In order to make a further research in the carbon monoxide oxidation, we formulated a second experiment under isothermal conditions. In this case an analysis of temperature sensitivity was performed.

Simulation conditions (RUN-3): Volumetric injection rate of 700 mL(SATD)/min with a composition of y$O_2$ : 0.21, y$H_2O$: 0.001 and y$N_2$: 0.789. Time dynamics for different isothermal simulations. The initial gas saturation was fixed on 0.7857, water saturation 0.05 and oil saturation on 0.1643. A more complete understanding on the effect of CO oxidation in the gas phase is evident in Figure 3.7, that maps different isothermal experiments and the temporal behavior.

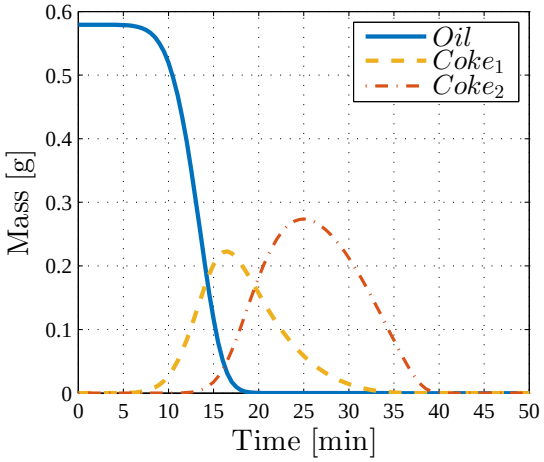


FIGURE 3.6: Oil and coke profiles for a combined RTO-isothermal experiment.

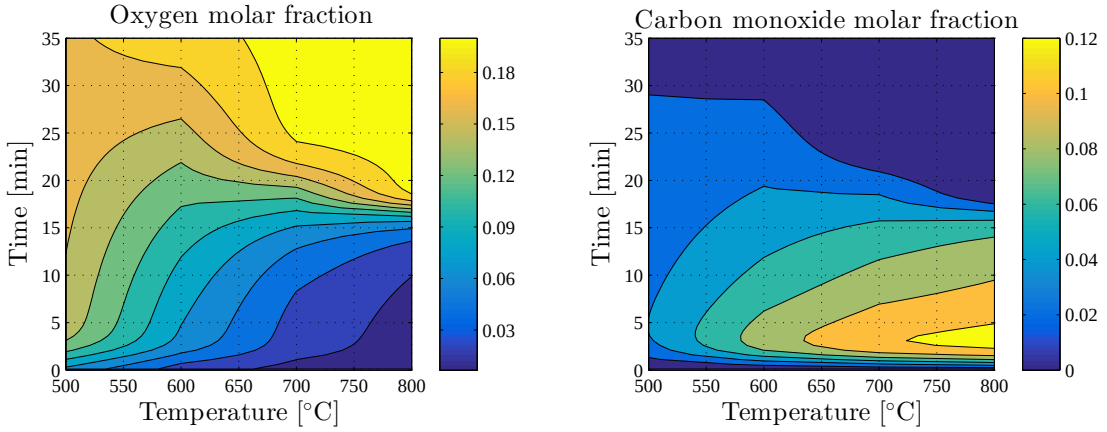


FIGURE 3.7: Oxidation profiles for isothermal experiments at 101.13kPa. Contour plots for $y_{O_2}$ and $y_{CO}$ molar fractions.

For example, at 700°C, the highest CO concentration is 0.1 (average mole fraction) between minute 2 and 7, then after minute 21 the combustion process ends. This behavior is also consistent with the oxygen profile, as the low concentration matches with the reaction zone before the first 7 minutes. In a more general analysis, it is possible to identify, that the most reactive zone corresponds to the higher temperature, which occurs faster and hence the maximum CO production is obtained for short time. This analysis is useful to determine operating conditions with the lowest CO concentration for environmental studies for an ISC project. They are also useful in determining the effect that the existence of gas-phase reactions may have on lab scale ISC experiments.

### 3.3.3 Single phase flow and halogen injection for CO oxidation

The purpose of this section is to illustrate how simple it is to management custom reactive species in the Toolbox. Two cases are specially designed to show what users can do with the simulator. RUN-4, includes new halogen species and reactions to the mechanism database in order to study reaction quenching in CO oxidation. RUN-5 introduces a different way to model the process with the perspective of chemical engineering.

Simulation conditions (RUN-4): Volumetric injection rate of 1L(SATD)/min with a composition of yCO: 0.08, y$O_2$: 0.14, y$H_2O$: 0.001, y$N_2$: 0.769, yI2: 0.01. Single phase flow (Sg=1) through a porous media under a heating rate of 5°C/min until 800°C, then isothermal operation on that temperature. The case represents a continuous reactor which reaches steady state. In the case without iodine, the compositions are yCO: 0.08, y$O_2$: 0.14, y$H_2O$: 0.001 and y$N_2$: 0.779.

Halogen addition, in this case iodine ($I_2$), suppresses carbon monoxide reactions in the reactor due to quenching of the hydroxyl radical ($OH^*$) mentioned before. The chemistry input file for CO oxidation with iodine considered GRI-Mech 3.0 and iodine species ($I_2, HI, I, IO, IOH$) and 28 reactions [77–79]. The Toolbox file FRUN.cti, includes the GRI-Mech 3.0 and also the halogen reactions. As a summary of important reactions, the mechanism begin with the dissociation of $I_2$, followed by hydrogen iodide formation (HI):

$$\mathrm{I_2 + M \longrightarrow I + I + M} \tag{R29}$$

$$\mathrm{I_2 + H \longrightarrow HI + I} \tag{R30}$$

$$\mathrm{H + I + M \longrightarrow HI + M} \tag{R31}$$

This scheme is defined by three-body reactions, where M is an unspecified collision partner that carries away excess energy to stabilize the molecules. Quenching of hydroxyl radicals is represented by the following reactions:

$$\mathrm{HI + H \longrightarrow I + H_2} \tag{R32}$$

$$\mathrm{HI + O \longrightarrow OH + I} \tag{R33}$$

$$\mathrm{HI + OH \longrightarrow I + H_2O} \tag{R34}$$

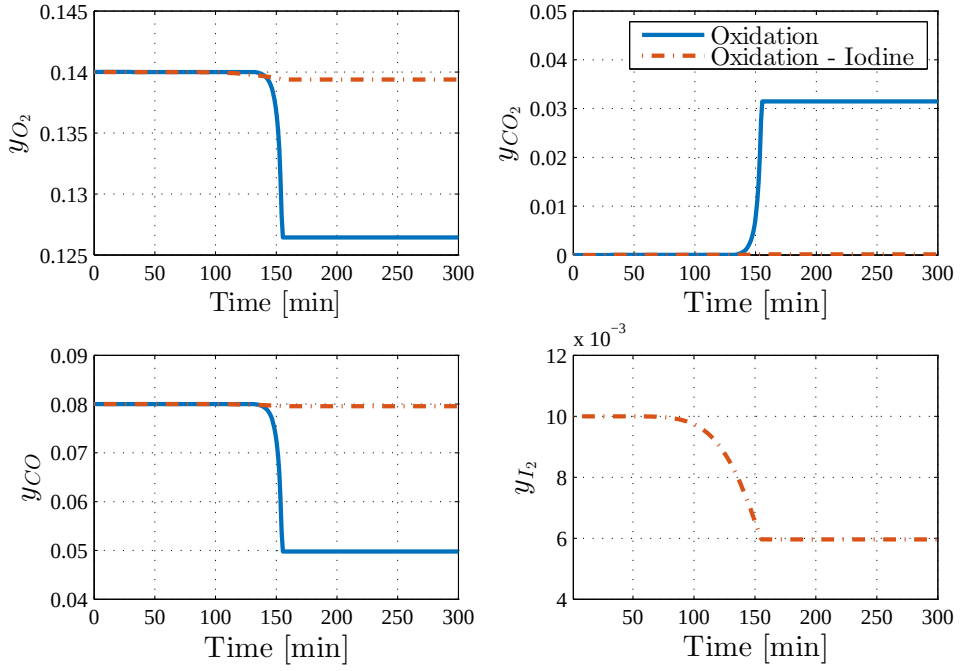


FIGURE 3.8: Influence of iodine injection in the oxidation of carbon monoxide. RTO experiment with a heating rate of 5°C/min.

The results of the simulation are presented in Figure 3.9. For a heating rate of 5°C/min, before the first 135 minutes, the temperature in the cell was not enough to activate the reactions, but then at 700°C the oxidation of CO begins, but only at 775°C (150min) the oxidation reaches 1% of CO consumption. The process goes to steady state when the isothermal operation at 800°C is performed. When iodine is injected to the cell, reaction quenching is strong enough to avoid the oxidation. The practical use of iodine injection on experimental setups is to control CO oxidation to study the influence of gas phase reactions in the quality and reliability of the measured data after the combustion process.

Finally, the previous results show that residence time is important to determine the progress of the reaction. In RUN-5, using chemical engineering theory, we find a way to model different residence times for the same experiment, just fixing different reactor volumes. So, the basic idea is to get the profile for the total reactor (0.12 m length), by simulating different lengths from 0 to 0.12 m with the same diameter. For example, the first reactor has a length of 0.01 m and the next reactor a length of $0.01 + \Delta Z$. We perform these sums until the total reactor length. This procedure is done for all the isothermal points. In this case we have single phase flow without halogens.

Simulation conditions (RUN-5): Volumetric injection rate of 700 mL(SATD)/min with a composition of yCO: 0.08, y$O_2$: 0.14, y$H_2O$: 0.001 and y$N_2$: 0.779. Single phase flow (Sg=1) through a porous media under isothermal condition. The case represents a continuous reactor which reaches steady state.

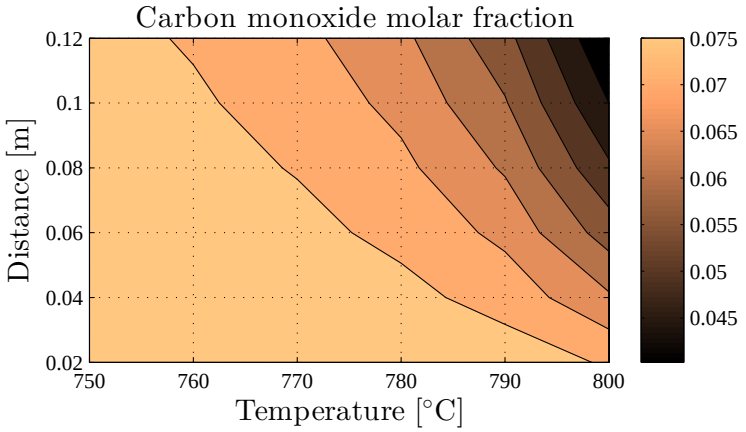


FIGURE 3.9: 1-Dimensional analysis for carbon monoxide oxidation in porous media.

From Figure 3.9, that presents results for the simulation of the isothermal oxidation for different residence times, it is possible to conclude that kinetic cell presents spatial compositions gradients, that can be important for certain operating conditions. This is a more generalized case of the steady state reached in RUN-4, because different isothermal experiments were carried out. For the analyzed temperature in the last case, if the temperature is 775°C the contour shows that at the exit of the kinetic cell, the CO concentration is about 0.07 (corresponding to the 1% of CO consumption). Additionally, as it is expected, higher temperatures about 800°C lead to more important gradients in the cell.

Also the new modeling approach leads to perform a more detailed analysis of the 1-Dimensional reactor. The chemical reactors perspective allows to model an ideal plug flow reactor as a sum in series of simple homogeneous 0-D reactors. This RUN-5 is the precursor of the reactor model developed in 4.

## 3.4 Conclusions

The main contribution of the work developed in this chapter is to provide a tool for study of chemical reactions in porous media coupled with in situ combustion reactions.

We provide an alternative that commercial software such as STARS do not have.

Carbon monoxide, as shown in the results is very sensible to operating conditions as flow, concentration ($O_2$ and CO partial pressures) and even more to temperature. Results show that changes in the CO profile, due to oxidation can be reached over 700°C at atmospheric pressure.

# Chapter 4

# Toolbox: Plug Flow Reactor

In Chemical engineering literature, a plug flow reactor (PFR) represents a continuous differential reactor, often used to obtain spatial profiles for a steady state reaction process. As a differential reactor, it is possible to model the space behavior with a sum of small reactors in series [80]. In analogy for the case of multiphase flow in porous media, each small reactor unit is essentially a kinetic cell.

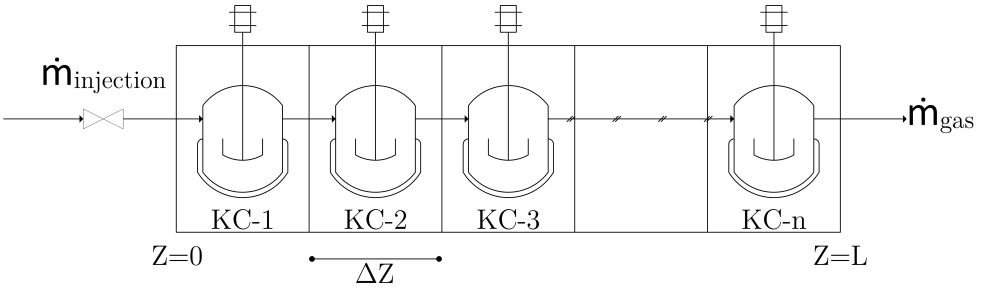


FIGURE 4.1: Schematic diagram for Plug Flow Reactor.

Figure 4.1 shows a scheme of the reactor modeling. The complete plug flow reactor is modeled as a number of small kinetic cells in series considering stationary oil/solid phases, and only gas flows through the reactor. As a way to improve the model, to obtain a more realistic behavior of the gradients of the process, is to include in the equations module one that considers the energy balance, including heat transfer by conduction and convection. With this PFR module in the Toolbox, it is possible to simulate steady

or unsteady RTO experiments, isothermal operations and also combustion fronts. Furthermore, it is an interesting modeling option, because the complexity is between that of a kinetic cell and a rigorous combustion process, which is described in Chapter 5.

Even though many authors [6, 8, 10, 11, 66] have studied 1-Dimensional kinetic cells and combustion tubes, this kind of modelling based on PFR reactors is not well implemented yet on ISC literature. Kinetic cells have been studied using reactor models based on compositional and full equation of state formulation, but most neglected the energy balance [8]. Complex software for computational fluid dynamics, such as ANSYS-Fluent, has been used to study homogeneity criteria on 1-D kinetic cell by using dimensionless Damköhler number [11]. However, this kind of software is not completely designed for this application, so the computational cost is really high for the simplest RTO experiment.

## 4.1 Governing equations

The plug flow reactor model is useful to study temperature gradients and composition in a kinetic cell. It is also useful to have quick estimates about the performance of a combustion tube. Equation notation is the same as Chapter 3, new terms are explained in each subsection. For more details about units and notation, refer to Symbols section.

The main assumptions are:

- Thermodynamic equilibrium.
- Pressure can be considered as uniform and constant, or constant pressure gradient ($\frac{\triangle P}{\triangle z}$) in a fixed value.
- Oil/water immiscible, non molecular diffusion.
- Oil is static, $viscosity \longrightarrow \infty$, and the viscosity does not change with temperature.
- No Darcy flow, gas flows with no accumulation, just like in the kinetic cell from Chapter 3.

The mole balance for each reactor is defined by

$$\frac{\partial N_i^k}{\partial t} = \sum_j F_{ij}^{in,k} - \sum_j F_{ij}^{out,k} + \sum_r \Lambda^{i,r}\gamma^{i,r}[=]\frac{mole}{time} \tag{4.1}$$

The grid blocks $k$ are in this case kinetic cells with the same volume as a normal block.

$$F_{ij}^{in,k} = F_{ij}^{out,k-1} \tag{4.2}$$

$$F_{ij}^{out,k} = F_{ij}^{in,k} + \sum_{r} \Lambda^{i,r}\gamma^{i,r} \tag{4.3}$$

Note that eventually $\frac{\partial N_i^k}{\partial t} = 0$ for gases (no accumulation). But the ODE algorithm still needs the derivative. Other methods as differential algebraic equation (DAEs) are also useful for this kind of equation.

For oil/solid phases:

$$\frac{\partial N_i^k}{\partial t} = \sum_{r} \Lambda^{i,r}\gamma^{i,r}[=]\frac{mole}{time} \tag{4.4}$$

The energy balance for gas phase in the plug flow reactor is similar to the kinetic cell, but in this case heat transfer by conduction is considered.

$$\sum_{i} N_i^k Cp_i^k \frac{dT^k}{dt} = \dot{Q}_{conv}^{in} - \dot{Q}_{conv}^{out} + \dot{Q}_{cond}^{in} - \dot{Q}_{cond}^{out} + \sum_{r} \Lambda^{i,r}\gamma^{i,r}\Delta H_{reac}^{r} \tag{4.5}$$

$$\dot{Q}_{conv}^{in} = \sum_{i} F_{i,gas}^{in,k} Cp_{gas}(T^{k-1} - T_{ref}) \tag{4.6}$$

$$\dot{Q}_{conv}^{out} = \sum_{i} F_{i,gas}^{out,k} Cp_{gas}(T^{k} - T_{ref}) \tag{4.7}$$

$$\dot{Q}_{cond}^{in} = -\alpha A \frac{(T^k - T^{k-1})}{\Delta z} \tag{4.8}$$

$$\dot{Q}_{cond}^{out} = -\alpha A \frac{(T^{k+1} - T^{k})}{\Delta z} \tag{4.9}$$

Boundary conditions for inlet ($k = 1$) and outlet ($k = NR$) are presented from Equation 4.10 to 4.13.

$$k = 1 \begin{cases} F_{ij}^{in,k} = F_{ij}^{injection} & (4.10) \\ T^{k-1} = T_{injection} & (4.11) \\ \dot{Q}_{cond}^{in} = 0 & (4.12) \end{cases}$$

$$k = NR \left\{ \;\; \dot{Q}_{cond}^{out} = 0 \right. \tag{4.13}$$

## 4.2 Model validation

The PFR model was validated in a controlled system without chemical reactions using the commercial software STARS. The main purpose was to verify that the gas flow and heat transfer capture the phenomena involved in the process. The model was based on the kinetic cell (already validated). Temperature profiles were important in order to validate the system dynamics, because the energy balance is highly dependent on mass conservation. If the temperature matches with STARS results, the mass transport is working as well.

In order to ensure that the gas flows freely in the system, a virtual high permeability was fixed over all the Cartesian domain. The parameters and STARS code can be found in appendix A. Dimensions of the reactor and main operating conditions are given in Table 4.1. The pressure drop is considered linear between the inlet and outlet pressure.

TABLE 4.1: Reactor parameters

| Parameter | Value |
|---|---|
| Cross sectional area | 0.062m × 0.062m |
| Reactor length | 1.204 m |
| Porosity | 0.378 |
| Volumetric air flow | 10 L(SATP)/min |
| Injection temperature | 500°C |
| Inlet Pressure (L=0m) | 105 kPa |
| Outlet Pressure (L=1.2m) | 101.13kPa |

Only heat transfer by conduction and convection was considered in a system with inert oil saturation of 0.05, and 0.95 for gas. So basically, the experiment consist in rock (and little portion of oil) heated by hot air injection.

Figure 4.2, shows the comparison of the results obtained with the toolbox and the STARS simulation. Initially the system is at ambient temperature and then, when hot air flows through the reactor, the rock takes the heat to increase slowly the local temperature. The results of the toolbox match very well the STARS profile for different simulation times. The process reaches steady state passed 400 min from injection.

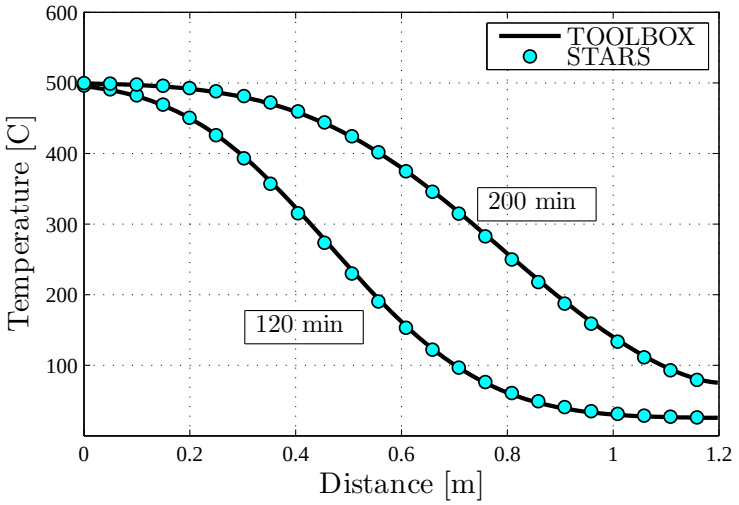


FIGURE 4.2: Plug Flow Reactor model validation. Comparison with STARS at 120 and 200 min.

## 4.3 Toolbox Applications

As in the previous chapter, this section illustrates the use of the plug flow reactor application of this toolbox with two examples. A 1-Dimensional kinetic cell and a combustion tube with a fixed pressure profile.

### 4.3.1 1-Dimensional kinetic cell

As we mentioned at the beginning of the chapter, this kind of reactor model can be used to simulate a 1-Dimensional combustion tube, but also a 1-Dimensional kinetic cell as long as oil flow can be neglected. In this toolbox application, we consider the same kinetic cell simulated before, but now we study the behavior under an unsteady RTO experiment.

Simulation conditions: Volumetric injection rate of 100 mL (SATD)/min with a composition of $yO_2$: 0.21 and $yN_2$: 0.79. Heating rate of 5°C/min until 800°C, then isothermal operation at 800°C. The initial gas saturation was fixed at 0.75, while oil saturation at 0.25. The pressure was kept constant at 1.01MPa.

For a comprehensive understanding of the experiment, we present in Figure 4.3, the oxygen molar fraction as a function of distance and time. At a heating rate of 5°C/min, when the temperature is enough to activate the oxidation reactions (above 275°C),

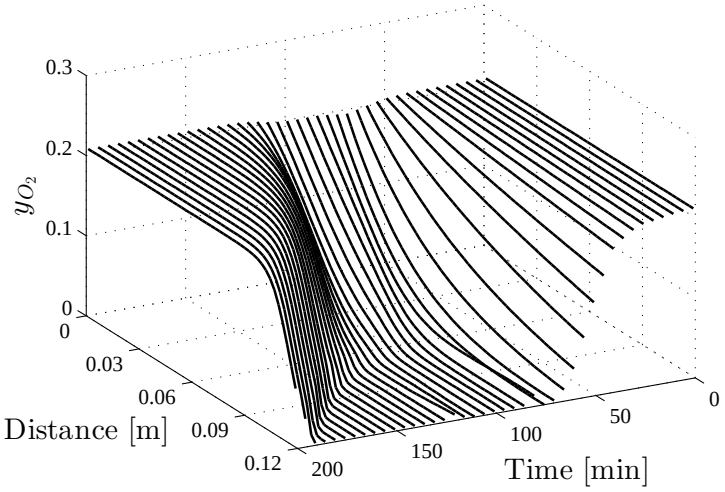


FIGURE 4.3: 3-Dimensional view of the oxygen mol fraction for a 5°C/min RTO experiment.

oxygen decreases almost to zero. After that, all the oxygen that is injected is consumed by the remaining oil in the kinetic cell. Basically, we identify two stages of the reaction presented in a two dimensional view in Figure 4.4. The first stage (Figure 4.4A) is before 100 min, at shorter times and lower temperatures, the reaction rates are low, so the oxygen in the system is in excess. As temperature increases, oxygen is strongly consumed. Eventually, after 100 min (Figure 4.4B), the concavity changes and the process is carried out in a different way.

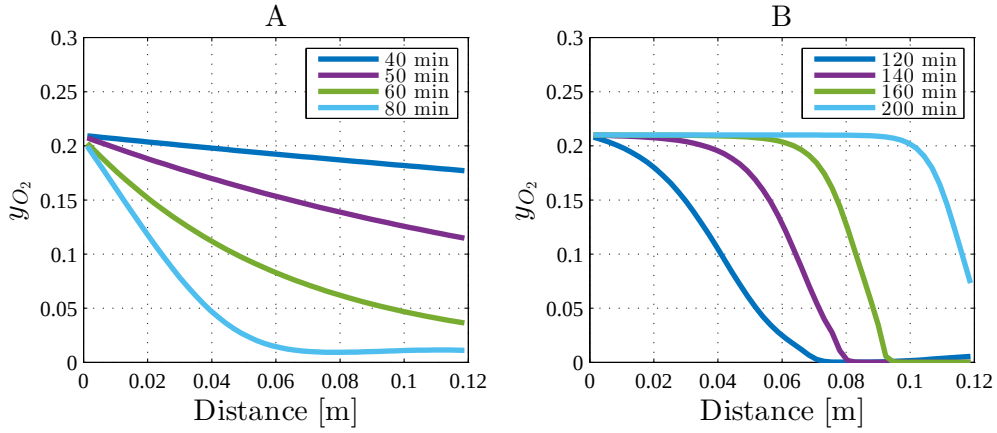


FIGURE 4.4: y$O_2$ profile for different times in the RTO experiment. A)times from 40 min to 80 min. B)times from 120 min to 200 min.

As Figure 4.5 shows, at the beginning of the experiment, oil was homogeneously consumed, due to the high oxygen concentration in kinetic cell. After that for high temperatures, all the injected oxygen reacts with oil and coke in the first 2 cm of the reactor.

The process after 100 min is piston like, so the oxygen moves through the cell following a clear combustion front.

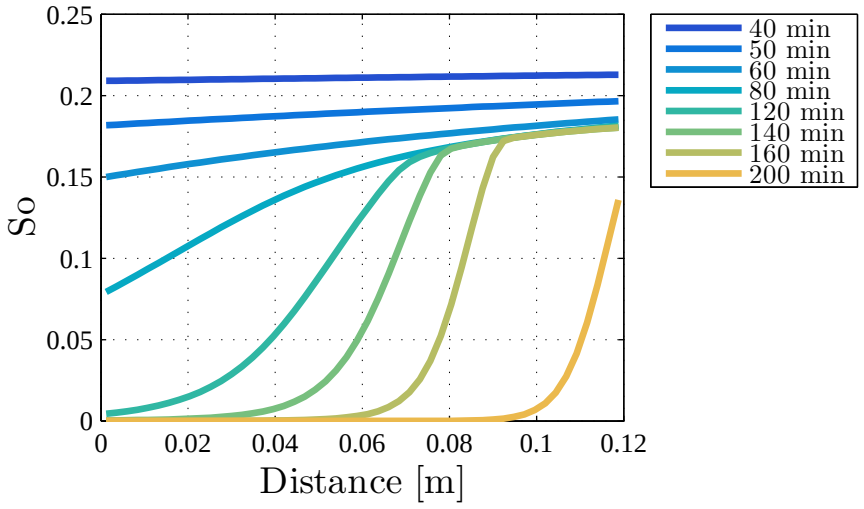


FIGURE 4.5: Oil saturation profile for different times in the RTO experiment.

For the experiment conditions, the combustion in the kinetic cell is not homogeneous. Different strategies as increase the air flow or saturate the core with low amount of oil can control gradients inside the cell, as described in [11].

### 4.3.2 Combustion tube with fixed pressure

This case of study corresponds to the same simulation from the PRF validation; but now, chemical reactions are activated in order to show the utility of the toolbox to have quick estimations of the combustion process. The result showed in Figure 4.6 , was obtained with the kinetic model and data from [73].

As we have shown in the validation section, the energy balance equation in the toolbox represents the main physic phenomena involved. In Figure 4.6, for short times, the toolbox matches the STARS profile, because the fixed pressure was quite similar for both simulators. But this is not the case at 200 min when the pressure profile along the tube departs from that of a linear pressure drop assumed as Figure 4.7 shows. While the difference is barely noticeable, this result indicates that pressure is important in order to have a good estimation of the reaction rate. Even with this profile deviation, is clear that we can perform quick combustion tube simulations, under the assumptions of the PFR. The computational speed in the calculations is really high (1 to 5 minutes with

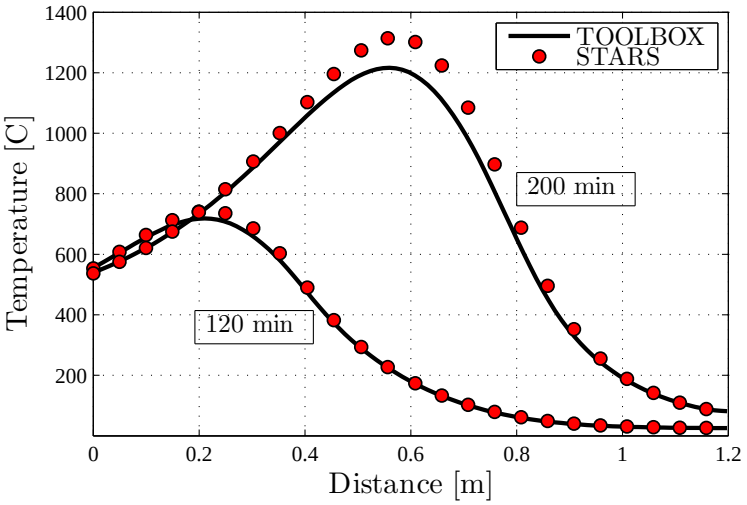


FIGURE 4.6: Combustion tube simulation with the PFR model. Comparison with STARS at 120 and 200 min.

100 reactors with Intel® Core™- i7 Processor), compared to complex combustion with energy, pressure and species balances that can take several hours in non-commercial academic developments.

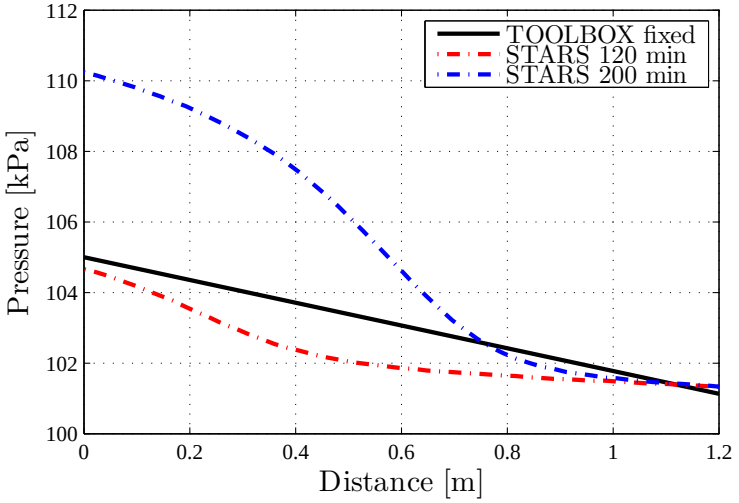


FIGURE 4.7: Pressure drop profile for the PFR model ($\frac{\Delta P}{\Delta z} = 3.32kPa \cdot m^{-1}$). Comparison with STARS at 120 and 200 min.

This case shows that calculation of the pressure profile along any experimental setups used to study the in-situ combustion process is important. This conclusion serves as a perfect introduction to Chapter 5, in which the application of the pressure equation and Darcy flow in the Toolbox is described.

## 4.4 Conclusions

The PFR model, designed for combustion in porous media, could be a very interesting and reliable alternative to model high permeable reactors (or low pressure drops) with low oil saturation.

With the toolbox it is possible to predict the behaviour of kinetic cells relaxing the assumption of perfect mixture. In this case, in agreement with that described in [11], 1-D profiles are evident for typical ISC experiments. This ability renders the toolbox particularly useful in the design experiments that avoid the gradients in the cell and simplify data analysis.

# Chapter 5

# Toolbox: Combustion Tube

The applications of the toolbox described so far, perform really well in the absence of pressure gradients. In this section a more complex model based on Darcy flow theory is developed. The emphasis of this Chapter is the combustion tube, and the mathematical model is based on multiphase flow in porous media equations that can be applied to study gradients in kinetic cells or any kind of reactor.

As mentioned before, lab scale experiments are mandatory in order to get estimations to design field operations [20]. The importance of the combustion tubes is due to their capability to study air and fuel requirements, combustion front stability and temperature and pressure profiles along the combustion tube. Combustion tubes cannot be directly correlated and scaled to reservoir; however, under similar conditions such as reservoir rock and fluids, the process could be quite similar in both cases. The problem between scales are related to the flow of fluids under reservoir heterogeneities and heat transfer. Many authors present more information about predictability and scale up of the process [23, 66, 81].

The experimental set-up for combustion tubes is usually as shown in Figure 5.1. Different sizes and configurations can be also founded in the literature. A normal experiment consists on an insulated stainless steel tube packed with native sand, clay and a mixture oil/water, where the ignition and propagation begins with electrical heating in the inlet zone until self propagation is reached. The advance of the combustion front can be recorded using a set of thermocouples uniformly spaced through the tube. Air injection

is controlled by fixing volumetric flow or inlet pressure as we discuss later. Finally outlet gases are analyzed and oil/water production measured.

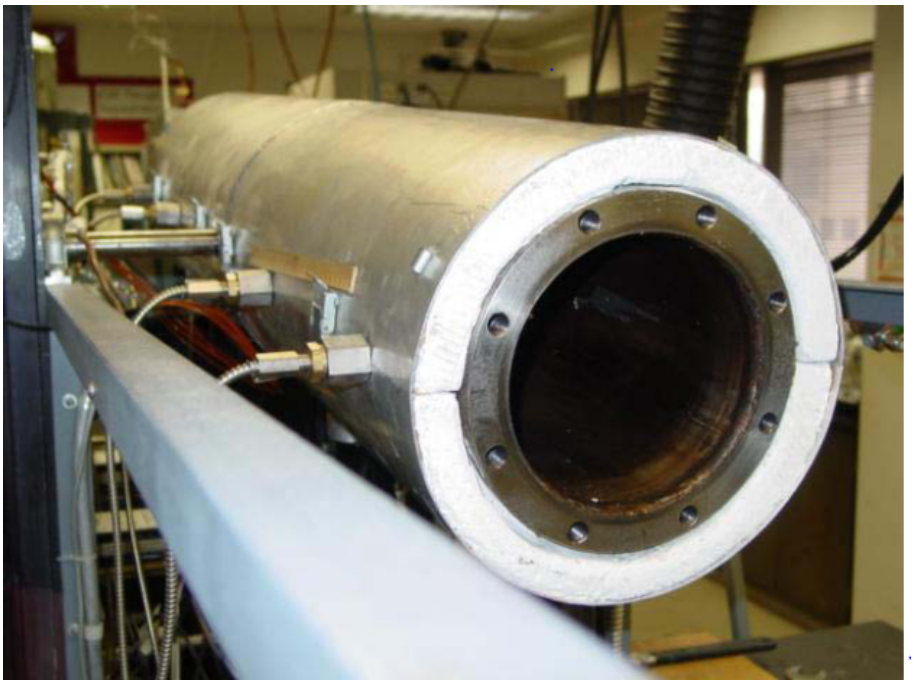

FIGURE 5.1: Combustion tube experiment [24].

Several studies of combustion tubes have been developed, trying to fit experiments and numerical simulations, sometimes without a good match. As we mentioned in the literature review in Chapter 1, the numerical simulation for this kind of process had a lot of analytical and predictive approaches. Robust simulators for laboratory studies as the work of Ramazan[59] , have been developed since 1990. Also new trends in porous media modelling appear in order to get reliable predictions, most of the new techniques include Coats and Crookston formulations [3, 51] as the model basis.

In a summary of studies for combustion tube simulations it is important to highlight the VCT (virtual combustion tube) developed by Krisensen with equation of state formulation and sophisticated numerical methods [25]. Artificial neural networks and intelligent methods were implemented by several authors in order to predict lab scale profiles and match experimenta data [82, 83]. Adaptive mesh refinement was conducted by Lovett [64] for compositional flow in porous media, while a new method based on a non-Arrheius reaction upscaling approach with streamlines simulation was performed by Zhu [23]. We present a novel approach, not described in the refereed literature, that model the combustion tube with a finite volume discretization.

## 5.1 Governing equations

### 5.1.1 Mass conservation

The model is based on transport in porous media theory without diffusional transport. We started from the formulation of the PFR reactor as is shown in Figure 5.2. In this case oil, gas and water can flow. The mole balance is presented as the temporal change of the concentration for specie $i$. Equation 5.1 considers the contribution of all phases $j$ for each species which is presented as the moles of specie over the reactor volume that includes rock matrix and fluid space. Equation notation remains the same as previous chapters and symbols table, new terms are explained as well.

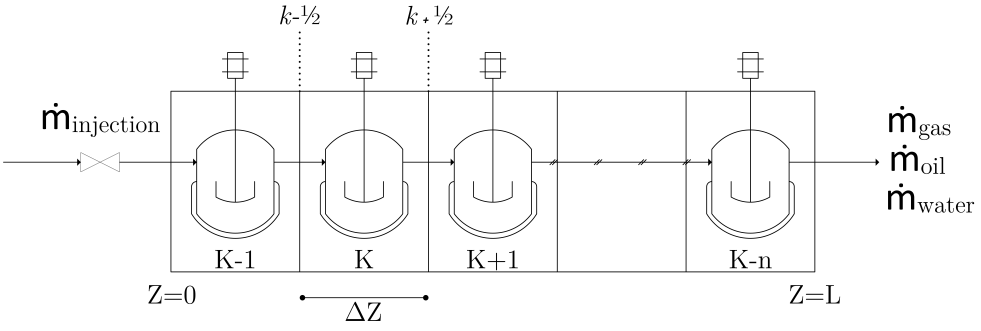


FIGURE 5.2: Schematic diagram for Combustion tube discretization.

The mole balance equation is given by:

$$\frac{\partial}{\partial t}(C_i) = \frac{\partial}{\partial t}(\sum_j \rho_j \phi S_j y_{i,j}) = -\nabla \cdot (\sum_j \rho_j u_j y_{i,j}) + \widehat{q_i}[=]\frac{moles}{TotalVol - time} = \frac{N_i}{V_T t} \quad (5.1)$$

Equation 5.1 must be solved for each species for all phases without any other simplification. A common procedure to solve this kind of partial differential equations is the finite volume method. First, we integrated Equation 5.1 over a control volume $\Omega$, and applying the divergence theorem change the volume integral into a surface integral for the convective term as is shown in Equation 5.2.

$$\int_\Omega \frac{\partial}{\partial t}(C_i) d\Omega = \int_S \nabla \cdot (\sum_j \rho_j u_j y_{i,j}) \cdot n dS + \int_\Omega \widehat{q_i} d\Omega \quad (5.2)$$

The discretization scheme and notation was shown in Figure 5.2, the problem in this thesis is one dimensional, the cross sectional area is the same as that of the combustion tube experiment and the finite volume is defined by the number of blocks in axial direction. The discretization nomenclature for the model is based on the computational fluid dynamics literature when the central block $k$, left block position is $k-1$, right position is $k+1$, left block interface is $k-1/2$ and right interface is $k+1/2$.

After the integration of the convective term, the equation is reduced to the balance between the inlet and oulet fluxes.

$$V_B \frac{\partial}{\partial t}(C_i^k) = \frac{\partial(N_i^k)}{\partial t} = -\left[\rho u y|_{k+1/2} - \rho u y|_{k-1/2}\right] A + q_i \tag{5.3}$$

where $V_B$ is the block volume, $q$ the moles generated/consumed per unit of time, $A$ the cross sectional area and $u$ the Darcy velocity.

At this point, the model was not complete, because in the convective term the velocity is an unknown variable. The porous media theory suggest that the velocity of phases should be evaluated with Darcy's equation, which transform the fluxes through the cross sectional area of the block interface into a function depending of the pressure gradient and the transport coefficient [84].

$$\frac{\partial(N_i^k)}{\partial t} = \left[ \left.\frac{\rho K k_r y}{\mu}\right|_{k+1/2} \left.\frac{\partial P}{\partial Z}\right|_{k+1/2} - \left.\frac{\rho K k_r y}{\mu}\right|_{k-1/2} \left.\frac{\partial P}{\partial Z}\right|_{k-1/2} \right] A + q_i \tag{5.4}$$

The pressure gradient can be approximated using central difference scheme (CDS),

$$\frac{\partial(N_i^k)}{\partial t} = \left.\frac{\rho K k_r y A}{\mu}\right|_{k+1/2} \frac{P_{k+1} - P_k}{\Delta Z} - \left.\frac{\rho K k_r y A}{\mu}\right|_{k-1/2} \frac{P_k - P_{k-1}}{\Delta Z} + q_i \tag{5.5}$$

As the pressure gradient is a negative term ($P_{k+1} < P_k$ and $P_k < P_{k-1}$), Equation 5.5 can be presented in the short form as

$$\frac{\partial(N_i^k)}{\partial t} = \sum_j \dot{N}_{i,j}^{in} - \sum_j \dot{N}_{i,j}^{out} + q_i \tag{5.6}$$

where $\dot{N}_{i,j}^{in}$ is the molar flow through the block face $k-1/2$ and $\dot{N}_{i,j}^{out}$ the molar flow through the block face $k+1/2$, for species $i$ in phase $j$. Notice that the formulation is very intuitive, because is the same mole balance as the kinetic cell (Equation 3.1) and PFR reactor (Equation 4.1), the only difference is the way to estimate the phase flow, in this case with Darcy.

$$\dot{N}_{i,j}^{in} = \left.\frac{-\rho_j K k_r y_i A}{\mu_j}\right|_{k-1/2} \frac{P_k - P_{k-1}}{\Delta Z} \tag{5.7}$$

$$\dot{N}_{i,j}^{out} = \left.\frac{-\rho_j K k_r y_i A}{\mu_j}\right|_{k+1/2} \frac{P_{k+1} - P_k}{\Delta Z} \tag{5.8}$$

The boundary conditions for the inlet and outlet flow are shown in Equations 5.9 and 5.10. The outlet flow ($Z = L$) calculated from Equation 5.10, presents a problem for pressure evaluated at $k+1$, because it is out of the reactor domain. A common strategy is to move this position to the edge $k+1/2$ and change the grid size to the half.

$$Inlet : \dot{N_i^{in}} = F_{k-1/2} = \dot{N}_{injection} \tag{5.9}$$

$$Outlet : \dot{N_i^{out}} = F_{k+1/2} = \left.\frac{\rho K k_r y}{\mu}\right|_{k=N} A \frac{P_{well} - P_{k=N}}{0.5\Delta Z} \tag{5.10}$$

### 5.1.2 Energy balance

The energy balance is given by:

$$\frac{\partial}{\partial t}\left((1-\phi)\,U_r + \phi \sum_{j=1}^{np} \rho_j S_j U_j\right) + \nabla \cdot \sum_{j=1}^{np} h_j \rho_j u_j + \nabla \cdot (-\alpha \nabla T) = q_{h,i} \tag{5.11}$$

The internal energy of the rock is $U_r$, $U_j$ is the internal energy of phase $j$, $h_j$ is the enthalpy of the phase $j$, $\alpha$ is the thermal conductivity and $q_{h,i}$ is a term that represents the thermal sinks and sources.

In order to get a more comprehensive model, it is possible to apply finite volume method as the mole balance for convective and conductive heat transfer, in this case the conduction is given by the temperature gradient and the derivative can be estimated by

CDS discretization. The mathematical procedure is the same as the mole conservation equation, for the generic block $k$ the equation is reduced to the difference between the inlet and outlet for both ways of heat transfer and also the generation of heat due to chemical reactions and external sources:

$$\sum_i \sum_j N_i^k C p_i^k \frac{dT^k}{dt} = \dot{Q}_{conv}^{in} - \dot{Q}_{conv}^{out} + \dot{Q}_{cond}^{in} - \dot{Q}_{cond}^{out} + \sum_r \Lambda^{i,r} \gamma^{i,r} \Delta H_{reac}^r \tag{5.12}$$

where the convective and conductive terms are calculated with Equations 5.13 to 5.16.

$$\dot{Q}_{conv}^{in} = \sum_i \sum_j \dot{N}_{i,j}^{in} h_j \Big|_{k-1/2} \tag{5.13}$$

$$\dot{Q}_{conv}^{out} = \sum_i \sum_j \dot{N}_{i,j}^{out} h_j \Big|_{k+1/2} \tag{5.14}$$

The outlet temperature is assumed to be the same as the block temperature, so in Equation 5.14, the temperature for enthalpy is evaluated at $k$.

$$\dot{Q}_{cond}^{in} = -\alpha A|_{k-1/2} \frac{(T^k - T^{k-1})}{\Delta z} \tag{5.15}$$

$$\dot{Q}_{cond}^{out} = -\alpha A|_{k+1/2} \frac{(T^{k+1} - T^k)}{\Delta z} \tag{5.16}$$

### 5.1.3 Pressure equation

In a control volume, it is known that the fluid occupies the whole porous volume, consequently a relation between volume and porosity can be obtained as shown in Equation 5.17 . The total volume conservation is an equation of state that bounds the evolution of mass and energy conservation. Therefore, looking for a concordance with the state equation, the pressure change can be expressed as a function of thermodynamic properties.

The change of the porous volume is a function of pressure, composition and temperature and can be related with the total volume using the next equations:

$$V_P = V_P(P, N_i, T) = \phi V_T \tag{5.17}$$

$$\frac{\partial V_P}{\partial t} = \frac{\partial \phi V_T}{\partial t} \tag{5.18}$$

with the assumption that the porosity is a function of pressure and that the temperature variation has a negligible effect, Equation 5.18 can be presented as follows,

$$\frac{\partial \phi V_T}{\partial t} = V_T \frac{\partial \phi}{\partial P} \frac{\partial P}{\partial t} \tag{5.19}$$

The same derivative expansion is applied to the porous volume,

$$\frac{\partial V_P}{\partial t} = \frac{\partial V_P}{\partial P} \frac{\partial P}{\partial t} + \frac{\partial V_P}{\partial T} \frac{\partial T}{\partial t} + \sum_{i=1}^{nc} \frac{\partial V_P}{\partial N_i} \frac{\partial N_i}{\partial t} \tag{5.20}$$

Equations 5.19 and 5.20 describe the change of the porous volume, so it is possible to equalize both expressions. After term grouping the resulting equation is presented as:

$$\left( V_T \frac{\partial \phi}{\partial P} - \frac{\partial V_P}{\partial P} \right) \frac{\partial P}{\partial t} = \frac{\partial V_P}{\partial T} \frac{\partial T}{\partial t} + \sum_{i=1}^{nc} \frac{\partial V_P}{\partial N_i} \frac{\partial N_i}{\partial t} \tag{5.21}$$

To get a more comprehensive and straightforward expression we define average properties. First, the average fluid compressibility is defined as

$$\widehat{c}_f = -\frac{1}{V_P} \frac{\partial V_P}{\partial P} \tag{5.22}$$

$$\widehat{c}_f = \sum_j S_j c_j \tag{5.23}$$

The rock compressibility is related to the porosity change due to pressure as

$$\widehat{c}_R = -\frac{1}{V_R} \frac{\partial V_R}{\partial P} = \frac{1}{1-\phi} \frac{\partial \phi}{\partial P} \tag{5.24}$$

$$\frac{\partial \phi}{\partial P} = \widehat{c}_R \left(1 - \phi\right) \tag{5.25}$$

The thermal expansion coefficient is defined as

$$\widehat{c}_T = \frac{1}{V_P} \frac{\partial V_P}{\partial T} \tag{5.26}$$

Including equations 5.22, 5.25 and 5.26 into Equation 5.21, we obtain:

$$\left(V_T\widehat{c}_R\left(1-\phi\right)+V_P\widehat{c}_f\right)\frac{\partial P}{\partial t}=V_P\widehat{c}_T\frac{\partial T}{\partial t}+\sum_{i=1}^{nc}\frac{\partial V_P}{\partial N_i}\frac{\partial N_i}{\partial t} \tag{5.27}$$

Finally, Equation 5.27 is divided by the total volume $V_T$ and then the porosity definition is applied.

$$\left(\widehat{c}_R\left(1-\phi\right)+\phi\widehat{c}_f\right)\frac{\partial P}{\partial t}=\phi\widehat{c}_T\frac{\partial T}{\partial t}+\frac{1}{V_T}\sum_{i=1}^{nc}\frac{\partial V_P}{\partial N_i}\frac{\partial N_i}{\partial t} \tag{5.28}$$

Notice that in this sequential formulation, to solve the pressure equation, the mole and energy balances need to have been previously calculated, so that the terms $\frac{\partial N_i}{\partial t}$ and $\frac{\partial T}{\partial t}$ are known. Also the term $\frac{\partial V_P}{\partial N_i}$ is the specific volume property for component $i$.

Now, in the discrete formulation, the balance for the reactor (or grid block $k$) is presented, where the total volume is changed by the block volume.

$$\left(\widehat{c}_R\left(1-\phi\right)+\phi\widehat{c}_f\right)\frac{\partial P^k}{\partial t}=\phi\widehat{c}_T\frac{\partial T^k}{\partial t}+\frac{1}{V_b}\sum_{i=1}^{nc}\frac{\partial V_P}{\partial N_i}\frac{\partial N_i^k}{\partial t} \tag{5.29}$$

## 5.2 Model validation

To ensure the validity of the new set of equations, we performed a comparison with STARS under a controlled system. To this, we designed a virtual experiment as simple as possible, in order to have the same variables and properties in both simulators. Basically, we took the case of study at the end of the Chapter 4, but now, the purpose was to match with the new approach the temperature, pressure and composition profiles. All the data required to simulate the process in this chapter and STARS inputs can be found in Appendix A.

First, we considered the oil as a stationary phase and then we show that the model is capable to predict oil mobility. There are mainly two options to make ignition in the combustion tube. The first one is to set electrical heating in the reactor inlet and also is possible to inject hot air to burn the oil. The electrical heating in this case is not a

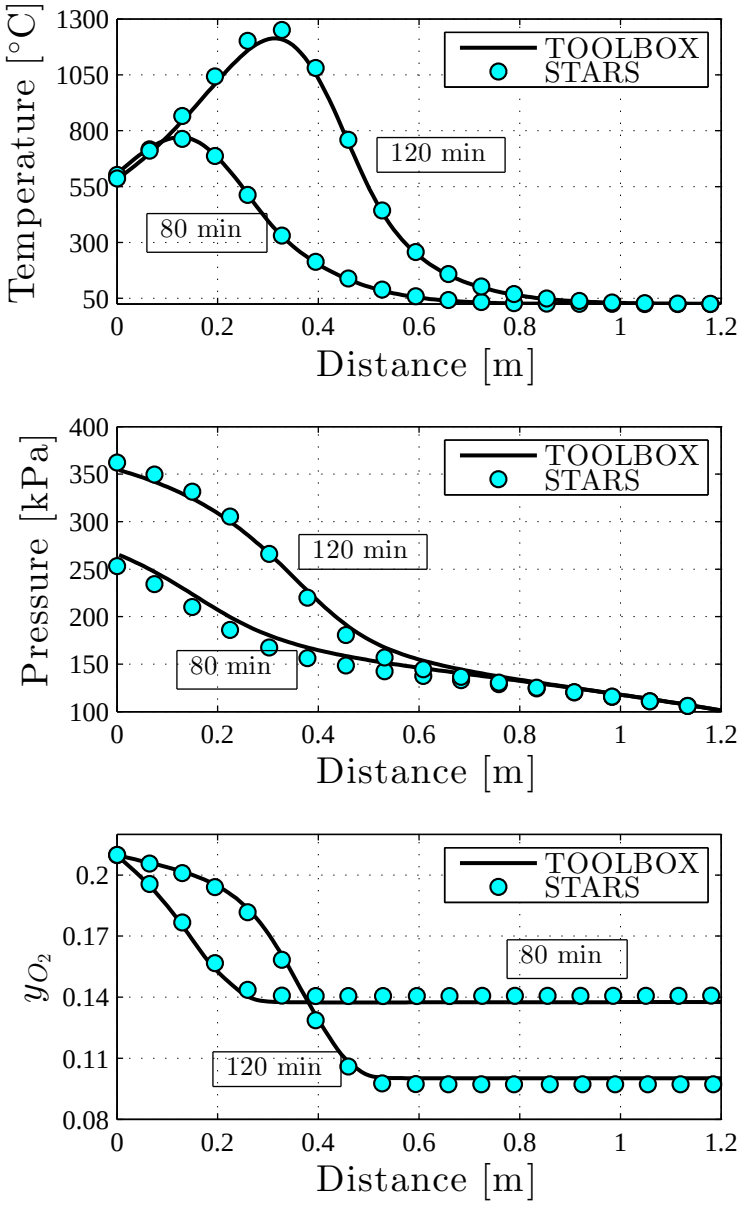


FIGURE 5.3: Combustion tube validation with STARS.

good option because the heater models that STARS uses were unknown which makes impossible any comparison. Contrary, the injection of the hot air at 500°C guarantees ignition and facilitates comparison.

Figure 5.3 presents the comparison with STARS for two simulation times. We got perfect match in most of the profiles and just negligible differences in the combustion front that could be caused by subtle differences in gases properties in STARS as some values for physical properties were not readily available in that software.

## 5.3 Toolbox Applications

As in the last two chapters, this section presents examples of applications of the combustion tube Toolbox. Due to the high complexity of the model and the large change of gradients along the tube, the computational cost, in this case, is between 10 to 12 hours with an Intel® Core™- i7 Processor.

### 5.3.1 Pressure analysis in the Combustion tube

Once we check the validity of the numerical solution, we proceeded to simulate a more realistic condition. In this case a normal combustion tube run packed with a mixture of heavy oil, sand and clay was simulated.

Simulation conditions: Volumetric injection rate of 10 L (SATD)/min with a composition of $yO_2$: 0.21 and $yN_2$: 0.79. The initial gas saturation was fixed on 0.75, while oil saturation on 0.25. The initial pressure and temperature were 101.13 kPa and 25°C respectively. Components properties, kinetic models and rock parameters are presented in Chapter 2.

In this kind of systems we have different options with the pressure equations. First, it is possible to fix the inlet pressure in an arbitrary value, but the inlet flow must be changed by the algorithm in order to secure mass and volume conservation. A more intuitive option is to fix the injection flow, then due to mass accumulation, the pressure will rise for the same reasons mentioned before. Depending on the study and the desire operating conditions, the pressure set-up should be carefully selected. In this particular case, an injection flow was fixed.

For regular combustion tube runs, once we have a combustion front, the heated oil moved by the pressure potential and allowed by the viscosity reduction, is accumulated just next to the combustion front. Oil accumulation is usually referred as an oil bank. The problem with highly viscous oils, which does not move properly at reservoir conditions, is related to the large oil bank formed, sometimes plugging the reactor. Figure 5.4 shows the oil saturation profiles for different process times. It is clear the large oil bank formed at 120 min, in which the saturation is three times more than the initial saturation.

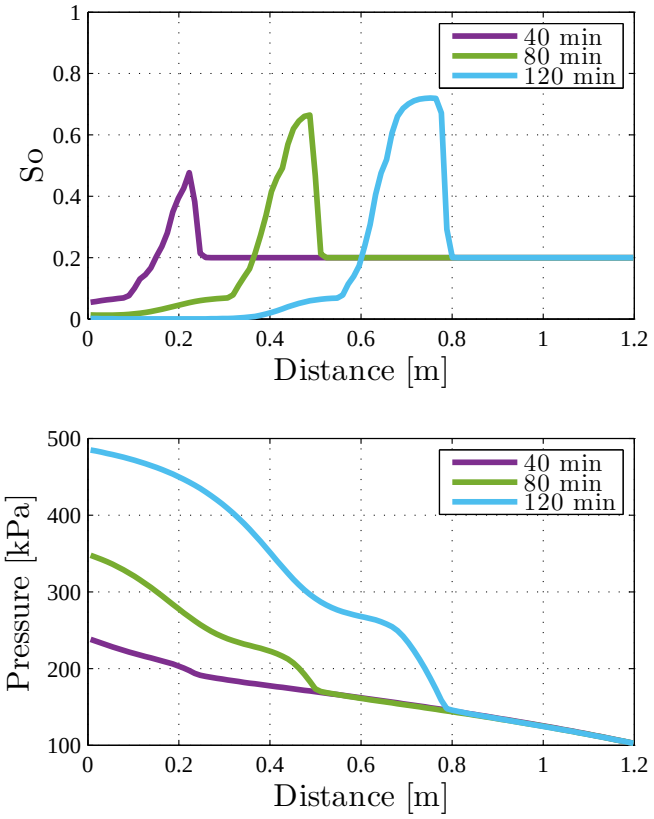


FIGURE 5.4: Oil saturation and pressure profiles for a combustion tube run.

As mentioned before in the modeling section, particularly in the pressure equation, the pressure is very sensitive to strong changes in the porous volume. With the results of Figure 5.4, we can set three zones in the pressure profile characteristic of longer times. The first zone for the 120 min profile, corresponding to the first 0.4 m of the tube, belongs to a free burned volume in which the gas will flow more easily due to the oil disappearance. The next 0.2 m of reactor corresponds to a transition zone, where the gas has to cross through the small volume due to the oil bank. This phenomena is the bottleneck of the flow and causes the major pressure increase. The last zone, from 0.8 m to 1.2 m, corresponds to the gas relief zone with an ideal linear pressure drop (normal in gases and steady state operations), in which no important phenomena occurs and also no flow restrictions appear until the discharge or well pressure.

### 5.3.2 Air injection with electrical heating

In order to simulate a regular combustion tube experiment, in this application air injection with electrical heating for ignition was performed. The electrical heaters are placed

in the first part of the packed tube, the idea is to set a controlled heating of the mixture in the same way as the kinetic cell, but in this case only the first grid blocks from the tube model are artificially controlled for a required time, the others follow the energy balance.

The chemical reactions used in this application are presented in equations R35 to R37 which are enough to represent LTO and HTO stages. The implementation of this short scheme is useful in order to get better computational efficiency.

$$Oil + 4.24O_2 \longrightarrow Coke_1 \tag{R35}$$

$$Coke_1 + 33.8O_2 \longrightarrow Coke_2 + 23.77CO_2 + 4.75CO + 22H_2O \tag{R36}$$

$$Coke_2 + 12.29O_2 \longrightarrow 8.56CO_2 + 6.161.73 + 8H_2O \tag{R37}$$

The kinetic data required to simulate the combustion process is presented in Table 5.1. The sign of the reaction enthalpy is already fixed in the code, for exothermic reactions the sign must be positive.

TABLE 5.1: Kinetic data used for the combustion tube simulation.

| Reaction | Frecuency factor $\left[\frac{1}{min \times kPa}\right]$ | Activation energy $\left[\frac{J}{mol}\right]$ | $\Delta H_{reac}\left[\frac{J}{mol}\right]$ |
|---|---|---|---|
| R1 | 0.01 | 22560 | $8.78\times10^5$ |
| R2 | 250 | 67525 | $7.04\times10^6$ |
| R3 | 220 | 87575 | $7.04\times10^6$ |

Simulation conditions: Horizontal tube test with air injection at 25°C, volumetric injection rate of 10L (SATD)/min with a composition of y$O_2$: 0.21 and y$N_2$: 0.79. The initial oil saturation was 0.2 and the physical properties for components and rock are the same as the previous applications (Appendix A and Chapter 2). The initial pressure and temperature were 101.13 k Pa and 25°C respectively. The heater set point was a linear ramped temperature with a rate of 20K/min for 30 minutes in the first 10 cm of the tube, then heaters are turned off for self-sustaining process.

The results for particular times of the combustion tube run are presented in Figure 5.5. The obtained profile shows the combustion front peak and a clear steam plateau zone. After the action of the heaters, the combustion front propagation is stable for the

time simulated. In this case the air flow at low temperature from the inlet is cooling the burned zone. It is important to notice that in the literature is possible to find combustion tube simulations with large temperature profiles [85], this is due to heat transfer problems. When the heat transfer properties of the rock matrix are low and heat losses are not considered, the temperature for the burned zone does not decrease normally.

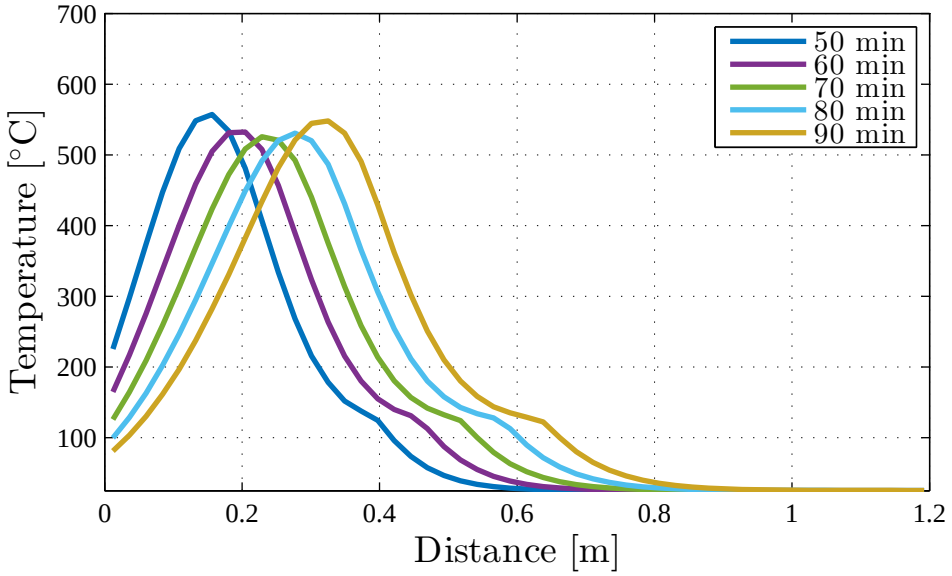


FIGURE 5.5: Temperature profile for cold air injection.

Figure 5.6 shows the variation of temperature with time. Only the maximum temperature is presented in order to follow the combustion front peak. The dashed line which increases linearly over the time is the ignition process with electrical heating. The set point is programmed to 625°C to make sure that combustion starts. After 30 minutes, the heaters are turned off and the chemical reactions for oil oxidation take control. The process after ignition takes other 30 minutes to reach a pseudo-stable state. It is possible to determine this pseudo-stable state from the figure, with an average temperature peak of 534.2°C.

## 5.4 Conclusions

The main contribution of this chapter is the implementation of the pressure equation. Many authors simulate the combustion tube only from the overall gas balance that leads several modeling problems [26, 63]. It is clear that gas phase is one of the most important

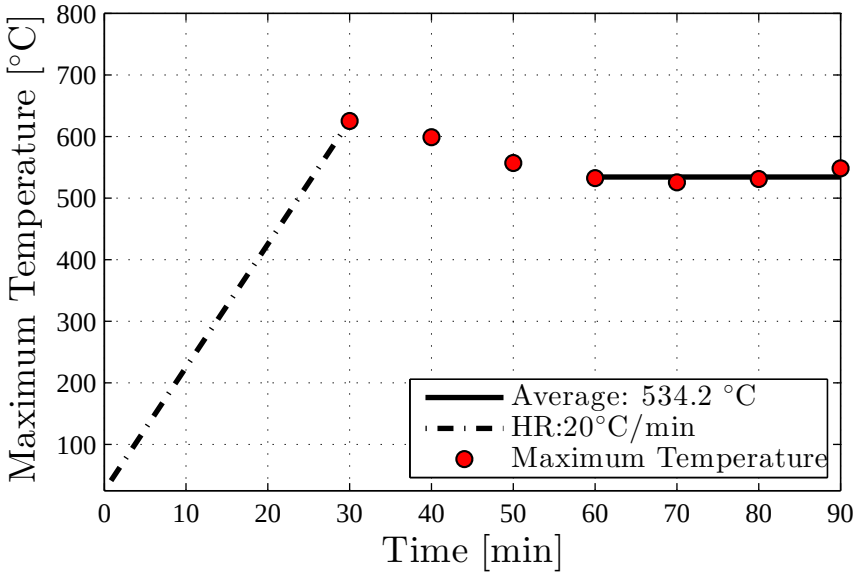


FIGURE 5.6: Temperature control in the combustion tube with electrical ignition process.

component responsible of the pressure changes in the combustion, but we demonstrate that oil plugging is also important, and the behavior is only captured with the volume conservation principle.

We develop a rigorous combustion tube model able to predict temperature, composition and pressure behavior, based on the chemical reactors approach and conservation equations. The toolbox is also designed to work for several operating conditions and ignitions process.

# Chapter 6

# Overall conclusions

The dissertation addressed the importance of the lab scale research in order to understand the process of in-situ combustion and the chemical reactions involved. The results in this document demonstrated the versatility and the utility of the simulation Toolbox developed to predict the ISC process on several experimental setups.

The main contributions of this work are the mathematical models based on fundamental laws and conservation equations, the facility of implement chemical reactions for ISC and gas phase reactions by Cantera coupling. Also the code and the algorithm structure to couple all the subroutines, source files and input data are considered an important contribution to the scientific community. The overall conclusions that fulfill the objectives of this study are summarized next.

- *To formulate a mathematical set of equations that describes the reactive flow in porous media.*

  We present a new way to model the reactive flow in porous media from the chemical engineering perspective, it was possible to show the features of the simulator from the simplest case in Chapter 3 (only gas flow without accumulation) to a more sophisticated formulation based on Darcy flow in Chapter 5. The kinetic cell, PFR and combustion tube models can be adapted to several configurations and operating conditions in order to predict and design the experiments.

- *To perform a sensitivity study of parameters and operating conditions for experimental setups.*

  The study of parameters and operating conditions was carried out in the toolbox applications as a way to prove that the simulator can reach realistic solutions for the different models and variables of the experiments. For the kinetic cell was found that concentration gradients can be important and it implies that the reactor is not working homogeneously, also some strategies to avoid the problem can be studied in the simulator such as increasing the air flow or saturate the core with low amount of oil.

  Regarding the application with Cantera, it was studied the oxidation regions for carbon monoxide, where at 700°C the gas phase reactions are activated properly and this process can be quenched using halogens as iodine.

  For combustion tubes, we are able to make ignition of the oil with a controlled heating and then track the process and determine if a stable combustion front is reached. Besides we also noticed that in horizontal configurations the reactor can be plugged up if the oil bank does not flow at the experiment conditions.

- *To apply numerical methods and algorithms to build the simulation toolbox, which suits the design alternatives.*

  Referring to the numerical methods, the ODE formulation and the choice of Matlab as programming language, allowed an excellent mathematical control of the solver variables that made easy the implementation of the GRI-MECH 3.0, because the values and rates for radicals and gas species are extremely low compared to the other variables, and also the control of the tolerances played an important roll in order to get a realistic solution in the less time possible.

  Also an important contribution of the toolbox formulation was the modeling of the phase equilibrium as a flash separation unit. This approach made easier the treatment of the equations for every specie and the programming of the module was more intuitive.

# Chapter 7

# Future work

Many problems and challenges encountered in this dissertation have been outside the scope. So, that can be the starting point for future works. We have grouped the most important aspects in different categories:

- **Toolbox applications.**

  Most of the effort in the present work was dedicated to the formulation of the reactor models and the programming of the algorithms, we would have liked to do more applications and variation to many important parameters. We provide the toolbox working for different reactors and conditions, so it would be desirable to perform specific and detailed works in only one single case of study, in this way the design and optimization of the process will be possible. In that order of ideas, we recommend to work with an oil well characterized in terms of physical properties, avoiding to take unreliable data from literature, which was one of the difficulties during this work. Some topics that would be interesting to address with the Toolbox are: wet combustion, gravity effects on vertical tubes and oil recovery. Our purpose was to bring a useful toolbox that can be applied to real reactors, so experimental matching would be interesting. Finally, future studies should consider the effects and amount of polluting gases such as $NO_x$, $H_2S$ and $CH_4$ during the ISC process. Cantera module can be used to predict the gas phase reactions for these species and also it is possible to improve the GRI-Mech 3.0 with custom reactions as we prove in Chapter 3.

- **Reactor models.**

  There is always a lot of work be carried out in the modeling part. Future studies should be focused in a more exclusive models specifically designed for the equipment in the laboratory. We also think that multidimensional models with heat losses are also important in the lab scale, because the environment in the reservoir and the lab are not the same. Regarding the pressure analysis in Chapter 5, we noticed that the toolbox should be adapted specifically to the pressure controllers in a real lab, in order to predict and match experimental results. Besides the gravity term in Darcy equation, should be included in future works in order to predict vertical combustion tubes and other reactors.

- **Numerical methods.**

  This is a challenging category and is currently one of the most investigated topic in reservoir simulation. The stiff ODE formulation based in numerical differentiation formulas, was used in the solver module of the toolbox with good accuracy in the solution, but in the case of the combustion tube, the computational cost was more than the expected. We also tried an implicit solution, using Newton iterations, with constant time stepping and grid size, but the ODE formulation was more efficient. We highly recommend the implementation in future works of adaptive mesh refinement and variable time step (based on the gradients). Other kind of improvement of the toolbox could be a better discretization scheme, to avoid possible numerical instabilities with the ODE solver.

# Appendix A

# STARS input data - Toolbox validation

The DAT input file that is required by STARS is presented below. This simulation was used in Chapters 4 and 5 to validate the results of the Toolbox. All the properties and experiment conditions, necessary to perform the simulations can be founded in this code. For more information of the syntax see STARS user's guide [42].

```
**————————————-INPUT-OUTPUT CONTROL————————————————————-
*TITLE1 'TOOLBOX VALIDATION WITH STARS - COMBUSTION TUBE '
*CASEID 'Model 1-cartesian'

**CHECKONLY
*INUNIT *LAB
*OUTUNIT *LAB

*WPRN *GRID *TIME
*WPRN *ITER *TIME
```

```
*OUTPRN *GRID *PRES *SW *SO *SG *TEMP *Y *X *MASS *SOLCONC
*OUTPRN *WELL *WELLCOMP
*OUTPRN *ITER *BRIEF


*WSRF *GRID *TIME
*WSRF *WELL 1
OUTSRF WELL MASS COMPONENT ALL
OUTSRF GRID PRES SG SO MASS SOLCONC SW TEMP X Y
OUTSRF SPECIAL MATBAL CURRENT 'CO'
OUTSRF SPECIAL MATBAL CURRENT 'CO2'
OUTSRF SPECIAL MATBAL CURRENT 'N2'
OUTSRF SPECIAL MATBAL CURRENT 'O2'
OUTSRF SPECIAL MATBAL CURRENT 'WATER'
OUTSRF SPECIAL MATBAL REACTION 'CO'
OUTSRF SPECIAL MATBAL REACTION 'CO2'
OUTSRF SPECIAL MATBAL REACTION 'O2'
OUTSRF SPECIAL MATBAL REACTION 'COKE1'
OUTSRF SPECIAL MATBAL REACTION 'COKE2'


*INTERRUPT *STOP


**———————-RESERVOIR DESCRIPTION———————————-
*GRID *CART 1 1 1204
**——IDIR *DOWN


*DI *CON 6.2
*DJ *CON 6.2
*DK *KVAR 1204*0.1
NULL CON 1
```

*POR *KVAR 1204*0.378

*PERMI *CON 10000

*PERMJ *CON 10000

*PERMK *CON 10000

PINCHOUTARRAY CON 1

*END-GRID

ROCKTYPE 1

**————————OTHER RESERVOIR PROPERTIES————————————-

*CPOR 0

*CTPOR 0

ROCKCP 1.20572 0

*THCONR 2.5833

THCONW 0.0

*THCONO 0.0

THCONG 0.0

*THCONS 0.0

**————————COMPONENT PROPERTIES————————————

** Model and number of components

** Model and number of components

** Model and number of components

** Model and number of components

** Model and number of components

** Model and number of components

** Model and number of components

MODEL 8 6 2 1

COMPNAME 'WATER' 'OIL' 'CO' 'CO2' 'N2' 'O2' 'COKE1' 'COKE2'

** ———- ——— —- ——— —- —- ———- ———-

CMM

0 0.5376 0.028 0.044 0.028 0.032 0.67304 0.17976

IDEALGAS

TCRIT

0 1472 -140.25 31.05 -146.95 -118.55

KV1

0 0

KV2

0 0

KV3

0 0

KV4

1 0

KV5

0 0

PRSR 101

TEMR 25

PSURF 101

TSURF 25

** Surface conditions

SURFLASH W O G G G G

** 'WATER' 'OIL' 'CO' 'CO2' 'N2' 'O2' 'COKE1' 'COKE2'

** ——- —— —- —— —- —- ——- ——-

CPG1

0 1138.8 29.987 16.864 30.288 27.627

CPG2

0 0 0 0 0 0

CPG3

0 0 0 0 0 0

CPG4

0 0 0 0 0 0

SOLID_DEN 'COKE1' 0.0326265 0 0

SOLID_DEN 'COKE2' 0.0088 0 0

SOLID_CP 'COKE1' 17.0 0

SOLID_CP 'COKE2' 17.0 0

MASSDEN

0 1.008E-3

CP

0 0

CT1

0 0

CT2

0 0

VISCTABLE

** temp

5 0 1636262

15 0 229374

25 0 54485.9

30 0 30000

48 0 10600

65 0 3000

100 0 290

150 0 32

200 0 7.5

250 0 2.7

300 0 1.0

325 0 0.75

350 0 0.60

375 0 0.50

400 0 0.47

425 0 0.41

450 0 0.36

475 0 0.315

500 0 0.28

525 0 0.25

550 0 0.22

2000 0 0.12

** 'WATER' 'OIL' 'CO' 'CO2' 'N2' 'O2' 'COKE1' 'COKE2'

** ——- —— —- —— —- —- ——- ——-

** Reaction 1: OIL + 4.24 O2 –¿ 1 'COKE1'

** Reaction specification

STOREAC

0.0 1.0 0.0 0.0 0.0 4.24 0.0 0.0

STOPROD

0.0 0.0 0.0 0.0 0.0 0.0 1.0 0.0

RPHASE

0 2 0 0 0 3 0 0

RORDER

0 1 0 0 0 1 0 0

**1/kPa-MIN

FREQFAC 0.01

** J/gmol

RENTH 1.597E6

**J/gmol

EACT 22560

RTEMUPR 5000

O2PP 'O2'

** 'WATER' 'OIL' 'CO' 'CO2' 'N2' 'O2' 'COKE1' 'COKE2'

** ——- —— —- —— —- —- ——- ——-

** R2: 'Coke1' + 33.8 O2 –¿ 4.75 CO + 23.77 CO2 + 22 WATER + 1'COKE2'

** Reaction specification

STOREAC

0.0 0.0 0.0 0.0 0.0 33.8 1.0 0.0

STOPROD

0 0.0 4.75 23.77 0.0 0.0 0.0 1.0

RPHASE

0 0 0 0 0 3 4 0

RORDER

0 0 0 0 0 1 1 0

**1/kPa-MIN

FREQFAC 250

** J/gmol

RENTH 1.28E7

**J/gmol

EACT 67525

RTEMUPR 5000

O2PP 'O2'

** 'WATER' 'OIL' 'CO' 'CO2' 'N2' 'O2' 'COKE1' 'COKE2'

** ——- —— —- —— —- —- ——- ——-

** Reaction 3: 'COKE2' + 12.29 O2 –¿ 1.73 CO + 8.56 CO2 + 8 Water

** Reaction specification

STOREAC

0.0 0.0 0.0 0.0 0.0 12.29 0.0 1.0

STOPROD

0 0.0 1.73 8.56 0.0 0.0 0.0 0.0

RPHASE

0 0 0 0 0 3 0 4

RORDER

0 0 0 0 0 1 0 1

**1/kPa-MIN

FREQFAC 220

** J/gmol

RENTH 4.85E6

**J/gmol

EACT 87575

RTEMUPR 5000

O2CONC 'CO2'

O2PP 'O2'

**————————————————-ROCK FLUID DATA————————————————

*ROCKFLUID

*RPT 1 *LININTERP *OILWET

** Sw Krw Krow Pcow

** —- — —- —-

*SWT

0.068 0.0000 1.0000 0

0.15 0.0077 0.8229 0

0.2 0.0200 0.7232 0

0.218 0.0259 0.6889 0

0.25 0.0381 0.6300 0

0.3 0.0619 0.5432 0

0.35 0.0915 0.4629 0

0.4 0.1268 0.3889 0

0.45 0.1679 0.3214 0

0.5 0.2148 0.2604 0

0.55 0.2674 0.2057 0

0.6 0.3258 0.1575 0

0.65 0.3899 0.1157 0

0.7 0.4598 0.0804 0

0.75 0.5354 0.0514 0

0.8 0.6168 0.0289 0

0.85 0.7040 0.0129 0

0.9 0.7969 0.0032 0

0.932 0.8956 0.0000 0

*SLT

** Sl Krg Krog Pcgo

** _ — —- —-

0.068 0.8975 0 0

0.1368 0.6845 1E-3 0

0.2 0.6233 0.0077 0

0.25 0.5429 0.0200 0

0.268 0.5154 0.0259 0

0.3 0.4681 0.0381 0

0.35 0.3989 0.0619 0

0.4 0.3352 0.0915 0

0.45 0.277 0.1268 0

0.5 0.2244 0.1679 0

0.55 0.1773 0.2148 0

0.6 0.1357 0.2674 0

0.65 0.0997 0.3258 0

0.7 0.0693 0.3899 0

0.75 0.0443 0.4598 0

0.8 0.0249 0.5354 0

0.85 0.0111 0.6168 0

0.9 0.0028 0.7040 0

0.932 1E-3 0.7969 0

1 0 0.8956 0

**————————————INITIAL CONDITION————————————————

*INITIAL

VERTICAL OFF

INITREGION 1

*PRES *CON 780

*TEMP *CON 25

*SW *CON 0.0

*SO *CON 0.2

*SG *CON 0.8

MFRAC_WAT 'WATER' CON 1

MFRAC_OIL 'OIL' CON 1

MFRAC_GAS 'O2' CON 0

```
MFRAC_GAS 'N2' CON 1
MFRAC_GAS 'CO2' CON 0
MFRAC_GAS 'CO' CON 0


**———————————-NUMERICAL CONTROL———————————
*NUMERICAL
MAXSTEPS 100000
MAXTEMP 5000
**DTMAX 0.1
DTMIN 0.000001
**————————————RECURRENT DATA————————————————-
*RUN
*TIME 0
DTWELL 0.01
*WELL 'MB-INJECTOR'
*WELL 'MB-PRODUCER'


**————— INJECTION PERIOD———————-


*PRODUCER 'MB-PRODUCER'
*OPERATE *MAX *BHP 780
** rad geofac wfrac skin
GEOMETRY K 0.5 1.0 1.0 0.0
PERF TUBE-END 'MB-PRODUCER'
** UBA ff Status Connection
1 1 1204 1.0 OPEN FLOW-TO 'SURFACE'


*INJECTOR 'MB-INJECTOR'
*TINJW 500
*PINJW 780
*INCOMP *GAS 0 0 0 0 0.79 0.21
```

*OPERATE *STG 10000

** rad geofac wfrac skin

GEOMETRY K 0.5 1.0 1.0 0.0

PERF TUBE-END 'MB-INJECTOR'

** UBA ff Status Connection

1 1 1 1.0 OPEN FLOW-FROM 'SURFACE'

*TIME 10

*TIME 79

*TIME 80

*TIME 81

*TIME 82

*TIME 83

*TIME 84

*TIME 85

*TIME 86

*TIME 87

*TIME 88

*TIME 89

*TIME 90

*TIME 91

*TIME 92

*TIME 93

*TIME 94

*TIME 95

*TIME 96

*TIME 97

*TIME 98

*TIME 99

*TIME 100

*TIME 101

*TIME 102

*TIME 103

*TIME 104

*TIME 211

*TIME 212

*TIME 213

*TIME 214

*STOP

# Appendix B

# Simulation Toolbox: Matlab code

The Matlab code that contains all the subroutines to characterize the process and reactor models is open to the academic community. It can be required by email to main authors Juan Hincapie (jufhincapieal@unal.edu.co) and Alejandro Molina (amolinao@unal.edu.co). The web page of the research group (Bioprocesos y Flujos Reactivos) contains the files in the repository.

The installation guide of Cantera can be found in: www.cantera.org

# Bibliography


[1] I. Nesterov, A. Shapiro, and E. Stenby. Numerical analysis of a one-dimensional multicomponent model of the in-situ combustion process. *Journal of Petroleum Science and Engineering*, 106:46–61, jun 2013. ISSN 09204105. doi: 10.1016/j.petrol.2013.03.022.

[2] O. Cazarez Candia and C. Centeno Reyes. Prediction of Thermal Conductivity Effects on in-situ Combustion Experiments. *Petroleum Science and Technology*, 27 (14):1637–1651, oct 2009. ISSN 1091-6466. doi: 10.1080/10916460802608958.

[3] Keith H Coats. In-Situ Combustion Model. *SPE Society of Pretroleum Engineers of AIME*, (December):533–554, 1980.

[4] R H Dean and L. L. Lo. Simulations of Naturally Fractured Reservoirs. *SPE international, society of pretroleum engineers*, (May), 1988.

[5] Alex Turta. *In Situ Combustion*. Elsevier Inc., first edit edition, 2013. doi: 10.1016/B978-0-12-386545-8.00018-X.

[6] Zeinab Khansari, Punitkumar Kapadia, Nader Mahinpey, and Ian D. Gates. A new reaction model for low temperature oxidation of heavy oil: Experiments and numerical modeling. *Energy*, 64:419–428, jan 2014. ISSN 03605442. doi: 10.1016/j.energy.2013.11.024.

[7] Partha S Sarathi. *In-Situ Combustion Handbook - Principles and Practices*. BDM-Oklahoma, Inc, Bartlesville, Oklahoma, 1998.

[8] Alexandre Lapene, Gerald Debenest, Michel Quintard, Louis M. Castanier, Margot G. Gerritsen, and Anthony R. Kovscek. Kinetics oxidation of heavy oil. 1. Compositional and full equation of state model. *Energy and Fuels*, 25(11):4886–4896, 2011. ISSN 08870624. doi: 10.1021/ef200365y.

[9] John D.M. Belgrave and R.Gordon Moore. A model for improved analysis of in-situ combustion tube tests. *Journal of Petroleum Science and Engineering*, 8(2):75–88, sep 1992. ISSN 09204105. doi: 10.1016/0920-4105(92)90046-4.

[10] J. Belgrave, R. Moore, M. Ursenbach, and D. Bennion. A comprehesive approach to in situ combustion modeling. *SPE Advance Technology Series*, 1:98–107, 1993.

[11] Sebastian López, Juan Hincapie, and Alejandro Molina. CFD evaluation of homogeneity in a kinetic cell used in the study of In Situ Combustion. page 6, Cartagena de Indias, Colombia, 2014. CCVII congreso Interamericano y Colombiano de Ingenieria Quimica.

[12] R. G. Moore, M. G. Ursenbach, C. J. Laureshen, J. D. M. Belgrave, and S. A. Mehta. Ramped Temperature Oxidation Analysis of Athabasca Oil Sands Bitumen. *Journal of Canadian Petroleum Technology*, 38(13):1–10, 1999. ISSN 0021-9487.

[13] Morten Rode Kristensen. *Development of Models and Algorithms for the Study of Reactive Porous Media Processes.* Thesis, Technical University of Denmark, 2008.

[14] R Castro, G Maya, D Mercado, M Trujillo, C Soto, H Pérez, and A Lobo. SPE 139199 Enhanced Oil Recovery (EOR) Status - Colombia. 2010. doi: 139199.

[15] E Tzimas. *Enhanced Oil Recovery using Carbon Dioxide in the European Energy System.* Number December. European commission, Petten, Neatherlands, 2005. ISBN 9279010441.

[16] William Lyons. *Working Guide to Reservoir Engineering.* Elsevier, 2010. ISBN 9781856178242. doi: 10.1016/B978-1-85617-824-2.00005-8.

[17] Zargon Oil & gas LTD. Oil explotation, 2016.

[18] Don Green and Paul Willhite. Enhanced Oil Recovery, 1988.

[19] M Prats. *Thermal recovery.* SPE of AIME,New York, NY, jan 1982.

[20] C. Gadelle and H. Bottia. The Role of laboratory in In situ Combustion project. *Features of exploration and development of unconventional hydrocarbons*, pages 37 –40, 2015.

[21] D.K. Banerjee. *Oil sands, Heavy oil & Bitumen. From recovery to refinery.* PennWell, Tulsa, Oklahoma, 2012. ISBN 9781593702601.

[22] Claude Gadelle, Jaques Burger, Charles Bardon, and Victor Machedon. Heavy-Oil Recovery by In-Situ Combustion - Two Field Cases in Rumania. *Journal of petroleum techno*, 1981.

[23] Zhouyuan Zhu. *Efficient simulation of thermal enhanced oil recovery processes.* Doctor of philosophy thesis, Stanford University, 2011.

[24] Jose Ramon Rodriguez. *Experimental and analytical study to model temperature profiles and stoichiometry in oxygen-enriched in situ combustion.* PhD thesis, Texas A&M University, 2004.

[25] Morten R. Kristensen, Margot G. Gerritsen, Per G. Thomsen, Michael L. Michelsen, and Erling H. Stenby. An Equation-of-State Compositional In-Situ Combustion Model: A Study of Phase Behavior Sensitivity. *Transport in Porous Media*, 76(2): 219–246, jul 2008. ISSN 0169-3913. doi: 10.1007/s11242-008-9244-6.

[26] Jaafar Sadiq. *An in-situ combustion simulator for enhanced oil recovery.* Tesis de doctorado, University of Salford, 1992.

[27] William E Brigham and Louis Castanier. In situ Combustion. In Edward D. Holstein, editor, *Petroleum Engineering Handbook*, volume 16, chapter 16, pages 1367–1398. Society of Petroleum Engineers, Dallas. TX, 2003. ISBN 978-1-55563-120-8.

[28] James Speight. *Enhanced recovery methods for heavy oil and tar sands.* Gulf publishing company, 2009. ISBN 9781933762258.

[29] Emuobonuvie Palmer-Ikuku. *Experimental study of in situ combustion with tetralin and metallic catalysts.* Master of science thesis, Texas A&M University, 2009.

[30] Mohammad Reza Fassihi, William E Brigham, and Henry Ramey. Reaction Kinetics of In-Situ Combustion : Part 2-Modeling. *SPE Society of Pretroleum Engineers of AIME*, pages 408–416, 1984.

[31] J. Burger and B. Sahuquet. Les méthodes thermiques de production des hydrocarbures. Chapitre 5 : Combustion "in situ". Pricipes et études de laboratoire. *Rev. Inst. Fr. Pét.*, 32(2):141–188, 1977. doi: 10.2516/ogst:1977010.

[32] Daulat Mamora. *Kinetics of in-situ combustion.* PhD thesis, 1993.

[33] Xiaomeng Yang and Ian D. Gates. Combustion Kinetics of Athabasca Bitumen from 1D Combustion Tube Experiments. *Natural Resources Research*, 18(3):193–211, apr 2009. ISSN 1520-7439. doi: 10.1007/s11053-009-9095-z.

[34] K. O. Adegbesan and J. K. Donnelly. Liquid Phase Oxidation Kinetics of Oil Sands Bitumen : Models for In Situ Combustion Numerical Simulators. *AICHE Journal*, 32(8):1242–1252, 1986.

[35] Nader Mahinpey, Aprameya Ambalae, and Koorosh Asghari. in Situ Combustion in Enhanced Oil Recovery (Eor): a Review. *Chemical Engineering Communications*, 194(8):995–1021, aug 2007. ISSN 0098-6445. doi: 10.1080/00986440701242808.

[36] J. D M Belgrave, R. G. Moore, and M. G. Ursenbach. Comprehensive kinetic models for the aquathermolysis of heavy oils. *Journal of Canadian Petroleum Technology*, 36(4):38–44, 1997. ISSN 00219487. doi: 10.2118/97-04-03.

[37] Bo Chen. Investigation of in-situ combustion kinetics using the isoconventional principle. (August), 2012.

[38] M. Cinar. Kinetics of crude-oil combustion in porous media interpreted using isoconversional methods. (August):377, 2011.

[39] N P Freitag and B Verkoczy. Low-Temperature oxidation of oils in terms of SARA fractions> why simple Reaction Models Don't Work. *Journal of Canadian Petroleum Technology*, 44:54–61, 1968. doi: 10.2118/05-03-05.

[40] ANSYS Fluent. ANSYS Fluids - CFD Simulation Software, Academic Research, 2016. URL http://www.ansys.com/Products/Fluids.

[41] OpenFOAM. OpenFOAM® - The Open Source Computational Fluid Dynamics (CFD) Toolbox, 2016. URL http://www.openfoam.com/.

[42] CMG. Advanced Process and Thermal Reservoir Simulator STARS, 2010.

[43] CHEMKIN. Reaction Design, 2013. URL http://www.reactiondesign.com/products/chemkin/chemkin-2/.

[44] D G Goodwin, H K Moffat, and Raymond L Speth. An object- oriented software toolkit for chemical kinetics, thermodynamics, and transport processes., 2016.

[45] H R Bailey and B K Larkin. Conduction-Convection in Underground Combustion. *SPE Society of Pretroleum Engineers of AIME*, 219:320–331, 1960.

[46] G.W. Thomas. A Study of Forward Combustion in a Radial System Bounded by Permeable Media. *Journal of Petroleum Technology*, 15(10):1145–1149, apr 1963. ISSN 0149-2136. doi: 10.2118/681-PA.

[47] B. S. Gottfried. A Mathematical Model of Thermal Oil Recovery. *SPE Society of Pretroleum Engineers of AIME*, SPE 1117:15, 1965.

[48] Earl J. Couch and Harold V. Rodriguez. Effects of Porosity Combustion and Permeability Fuel Consumption on. *SPE Society of Pretroleum Engineers of AIME*, SPE 2873:11, 1970.

[49] SM Farouq-Ali. Multiphase, Multidimensional Simulation of in-situ Combustion. *SPE Society of Pretroleum Engineers of AIME*, Paper SPE:11, 1977.

[50] U. K. Acharya and W. H. Somerton. Theoretical study of in-situ combustion in thick inclined oil reservoirs. *SPE Society of Pretroleum Engineers of AIME*, SPE 7967:16, 1979.

[51] R.B. Crookston, W.E. Culham, and W.H. Chen. A numerical simulation model for thermal recovery processes. *SPE Society of Pretroleum Engineers of AIME*, SPE 6724:22, 1979.

[52] Janusz. W. Grabowski, Paul K. Vinsome, Ran C. Lin, Alda Behie, and Barry Rubin. A fully implicit general purpose finite-difference thermal model for in situ combustion and steam. *SPE Society of Pretroleum Engineers of AIME*, SPE 8396: 14, 1979.

[53] L. C. Young and R. E. Stephenson. A Generalized Compositional Approach for ReseIVoir Simulation. *SPE international, society of pretroleum engineers*, (October), 1983.

[54] M Anis, M.K. Hwang, and A.S. Odeh. A Sensitivity Study of the Effect of Parameters on Results From an In-Situ Combustion Simulator. *SPE Society of Pretroleum Engineers of AIME*, (April):259–264, 1983.

[55] B. Rubin and W. L. Buchanan. A General Purpose Thermal Model. *SPE international, society of pretroleum engineers*, page 13, 1985.

[56] M.O. Onyekonwu, K. Pande, H.J. Ramey, and W.E. Bringham. Experimental ans Simulation Studies of Laboratory In-Situ Combustion Recovery. *SPE international, society of pretroleum engineers*, SPE 15090:14, 1986.

[57] J.F. Genrich and G.a. Pope. A Simplified Performance-Predictive Model for In-Situ Combustion Processes. *SPE Reservoir Engineering*, 3(02):410–418, apr 1988. ISSN 0885-9248. doi: 10.2118/14242-PA.

[58] Pierre A. Le Thiez and Patrick A Lemonnier. An In-Situ Combustion Reservoir Simulator With a New Representation of Chemical Reactions. *SPE Reservoir Engineering*, (August):285–292, 1990.

[59] R. Ocalan and M. V. Kok. In situ combustion model development and its applications for laboratory studies. *Fuel*, 74(11):1632–1635, nov 1995. ISSN 00162361. doi: 10.1016/0016-2361(95)00162-X.

[60] I.Yucel Akkutlu and Yanis C. Yortsos. The dynamics of in-situ combustion fronts in porous media. *Combustion and Flame*, 134(3):229–247, aug 2003. ISSN 00102180. doi: 10.1016/S0010-2180(03)00095-6.

[61] I Yucel Akkutlu and Yannis C Yortsos. The Effect of Heterogeneity on In-Situ Combustion : Propagation of Combustion Fronts in Layered Porous Media. *SPE international, society of pretroleum engineers*, SPE 75128(May 2002):13–17, 2005.

[62] Zhenshuo Liu. *Optimization of in-situ combustion: Maximizing production and reducing CO2 footprint.* PhD thesis, UNIVERSITY OF SOUTHERN CALIFORNIA, 2011.

[63] M.S.K. Youtsos and E. Mastorakos. Numerical simulation of thermal and reaction waves for in situ combustion in hydrocarbon reservoirs. *Fuel*, 108:780–792, jun 2013. ISSN 00162361. doi: 10.1016/j.fuel.2013.02.034.

[64] Sean Lovett, Franck Monmont, and Nikolaos Nikiforakis. An experimentally-based in-situ combustion model with adaptive meshing. *Combustion and Flame*, oct 2014. ISSN 00102180. doi: 10.1016/j.combustflame.2014.09.018.

[65] David G Goodwin, Harry K Moffat, and Raymond L Speth. Cantera: An Object-oriented Software Toolkit for Chemical Kinetics, Thermodynamics, and Transport Processes. \url{http://www.cantera.org}, 2016.

[66] Mohammad Bazargan. Measurement of in-situ combustion reaction kinetics with high fidelity and consistent reaction upscaling for reservoir simulation. (May), 2014.

[67] Crane Company. Flow of fluids throuh valves, fittings and pipe. Technical Paper No. 410, 1988.

[68] MATLAB. MathWorks – MATLAB and Simulink, 2016.

[69] Lawrence F Shampine and Mark W Reichelt. The matlab ode suite. *SIAM journal on scientific computing*, 18(1):1–22, 1997.

[70] M Cinar, L M Castanier, and a R Kovscek. Isoconventional Kinetic Analysis of the Combustion of Heavy Hydrocarbons. (2):4003–4015, 2009.

[71] Mohammad Bazargan, Alexandre Lapene, Bo Chen, Louis M. Castanier, and Anthony R. Kovscek. An induction reactor for studying crude-oil oxidation relevant to in situ combustion. *Review of Scientific Instruments*, 84(7), 2013. ISSN 00346748. doi: 10.1063/1.4815827.

[72] L. M. Gaviria. *Kinetic parameters for in situ combustion of Chichimene crude oil*. Master's thesis, Universidad Nacional de Colombia - Sede Medellin, 2016.

[73] B. Dechelette, J. R. Christensen, O. Heugas, G. Quenault, and J. Bothua. Air injection - Improved determination of the reaction scheme with ramped temperature experiment and numerical simulation. *Journal of Canadian Petroleum Technology*, 45(1):41–47, 2006. ISSN 00219487. doi: 10.2118/06-01-03.

[74] Morten R. Kristensen, Margot G. Gerritsen, Per G. Thomsen, Michael L. Michelsen, and Erling H. Stenby. Efficient integration of stiff kinetics with phase change detection for reactive reservoir processes. *Transport in Porous Media*, 69(3):383–409, jan 2007. ISSN 0169-3913. doi: 10.1007/s11242-006-9079-y.

[75] Priyanka Jain, Erling H Stenby, and Nicolas Von Solms. Compositional Simulation of In-Situ Combustion EOR : A Study of Process Characteristics. *SPE Improved Oil Recovery Symposium*, pages 1–18, 2010. doi: 10.2118/129869-MS.

[76] J. Burger and B. Sahuquet. Chemical Aspects of in-Situ Combustion - Heat of Combustion and Kinetics. *Society of Petroleum Engineers of AIME Journal*, 12(5): 410–422, 1972. ISSN 0197-7520. doi: 10.2118/3599-PA.

[77] Franz Winter, Christian Wartha, Gerhard Löffler, and Hermann Hofbauer. The NO and N2O formation mechanism during devolatilization and char combustion under fluidized-bed conditions. *Symposium (International) on Combustion*, 26(2): 3325–3334, 1996. ISSN 00820784. doi: 10.1016/S0082-0784(96)80180-9.

[78] Franz Winter, Gerhard Löffler, Christian Wartha, Hermann Hofbauer, Fernando Preto, and Edward J. Anthony. The NO and N20 Formation Mechanism under Circulating Fluidized Bed Combustor Conditions: from the Single Particle to the Pilot-Scale. *The Canadian Journal of Chemical Engineering*, 77, 1999.

[79] F Winter, C Wartha, and H Hofbauer. Relative importance of radicals on the N{sub 2}O and NO formation and destruction paths in a quartz CFBC. *Journal of Energy Resources Technology, Transactions of the ASME*, 121(2):131–136, 1999. ISSN 01950738.

[80] H. Scott Fogler. *Elements of chemical reaction engineering.* 1999. ISBN 0139737855. doi: 10.1016/0009-2509(87)80130-6.

[81] A R Kovscek, L M Castanier, and M G Gerritsen. Improved predictability of in-situ combustion enhanced oil recovery. *SPE Reservoir Evaluation & Engineering*, 16(02):172 – 182, 1999. doi: 10.2118/165577-PA.

[82] Yogesh Bansal. *Conducting in-situ combustion tube experiments using artificial neural networks.* PhD thesis, Pennsylvania State University, 2009.

[83] Mohammad Ali Ahmadi, Mohammad Masoumi, and Reza Askarinezhad. Evolving Smart Model to Predict the Combustion Front Velocity for In Situ Combustion. *Energy Technol.*, pages 1–9, 2015. ISSN 21944288. doi: 10.1002/ente.201402104.

[84] Zhangxin Chen, Guanren Huan, and Yuanle Ma. *Computational Methods for Multiphase Flows in Porous Media.* 2006. ISBN 0898716063.

[85] Olufolake Olubusayo Ogunbanwo, Margot Geertrui Gerritsen, and Anthony Robert Kovscek. Uncertainty Analysis on In-Situ Combustion Simulations Using Experimental Design. *SPE Western Regional Meeting*, 2013. doi: 10.2118/153887-MS.